Deoxyxylulose 5-Phosphate Synthase Controls Flux through the Methylerythritol 4-Phosphate Pathway in Arabidopsis[1][C][W][OPEN]

Louwrance P. Wright*, Johann M. Rohwer, Andrea Ghirardo, Almuth Hammerbacher, Miriam Ortiz-Alcaide, Bettina Raguschke, Jörg-Peter Schnitzler, Jonathan Gershenzon, and Michael A. Phillips*

Department of Biochemistry, Max Plank Institute for Chemical Ecology, 07745 Jena, Germany (L.P.W., A.H., B.R., J.G.); Department of Biochemistry, Stellenbosch University, 7602 Stellenbosch, South Africa (J.M.R.); Research Unit Environmental Simulation (EUS), Institute of Biochemical Plant Pathology, Helmholtz Zentrum, 85764 Neuherberg, Germany (A.G., J.-P.S.); and Plant Metabolism and Metabolic Engineering Program, Centre for Research in Agricultural Genomics (Consorci CSIC-IRTA-UAB-UB), 08193 Bellaterra, Barcelona, Spain (M.O., M.A.P.)

ORCID IDs: 0000-0001-5998-6079 (L.P.W.); 0000-0001-7276-119X (M.A.P.).

The 2-C-methylerythritol 4-phosphate (MEP) pathway supplies precursors for plastidial isoprenoid biosynthesis including carotenoids, redox cofactor side chains, and biogenic volatile organic compounds. We examined the first enzyme of this pathway, 1-deoxyxylulose 5-phosphate synthase (DXS), using metabolic control analysis. Multiple Arabidopsis (*Arabidopsis thaliana*) lines presenting a range of DXS activities were dynamically labeled with $^{13}CO_2$ in an illuminated, climate-controlled, gas exchange cuvette. Carbon was rapidly assimilated into MEP pathway intermediates, but not into the mevalonate pathway. A flux control coefficient of 0.82 was calculated for DXS by correlating absolute flux to enzyme activity under photosynthetic steady-state conditions, indicating that DXS is the major controlling enzyme of the MEP pathway. DXS manipulation also revealed a second pool of a downstream metabolite, 2-C-methylerythritol-2,4-cyclodiphosphate (MEcDP), metabolically isolated from the MEP pathway. DXS overexpression led to a 3- to 4-fold increase in MEcDP pool size but to a 2-fold drop in maximal labeling. The existence of this pool was supported by residual MEcDP levels detected in dark-adapted transgenic plants. Both pools of MEcDP are closely modulated by DXS activity, as shown by the fact that the concentration control coefficient of DXS was twice as high for MEcDP (0.74) as for 1-deoxyxylulose 5-phosphate (0.35) or dimethylallyl diphosphate (0.34). Despite the high flux control coefficient for DXS, its overexpression led to only modest increases in isoprenoid end products and in the photosynthetic rate. Diversion of flux via MEcDP may partly explain these findings and suggests new opportunities to engineer the MEP pathway.

Most isoprenoids in plants are derived from the plastid-localized 2-C-methylerythritol 4-phosphate (MEP) pathway (Fig. 1), which produces isopentenyl diphosphate (IDP) and dimethylallyl diphosphate (DMADP), the common precursors of monoterpenes (Croteau, 1987), diterpenes, carotenoids (Ruiz-Sola and Rodríguez-Concepción, 2012), the prenyl chains of chlorophyll and plastoquinones, and some sesquiterpenes (Dudareva et al., 2005). Many volatile compounds that play roles in plant defense are also made from precursors supplied by the MEP pathway (Gershenzon and Dudareva, 2007). The cytosol-localized mevalonate pathway of plants also produces IDP and DMADP as precursors for sterol biosynthesis and protein farnesylation. A limited exchange of common intermediates between the two pathways has been observed in several plant systems (Bick and Lange, 2003; Hemmerlin et al., 2003; Laule et al., 2003; Flügge and Gao, 2005), but this exchange is not capable of rescuing a pharmacological block in either pathway (Laule et al., 2003; Rodríguez-Concepción et al., 2004). Indeed, the identification of several Arabidopsis (*Arabidopsis thaliana*) mutants of the MEP pathway based on defects in chloroplast development (Gutiérrez-Nava et al., 2004; Guevara-García et al., 2005) was facilitated by the lack of substantial exchange. Hence, the MEP pathway is effectively the only source of precursors for essential plastid isoprenoids.

Since the relatively rapid elucidation of the steps in the MEP pathway in the late 1990s and early 2000s, efforts have turned to understanding pathway regulation.

[1] This work was supported by a Ramón y Cajal contract from the Spanish Ministry of Science and Innovation (contract no. RYC–2010–05759 to M.A.P.), a research fellowship from the Deutsche Forschungsgemeinschaft (PH 179/1–1 to M.A.P.), and a Max Planck Society-Fraunhofer Society Cooperation (to L.P.W. and J.G.).

* Address correspondence to michael.phillips@cragenomica.es and lwright@ice.mpg.de.

The author responsible for distribution of materials integral to the findings presented in this article in accordance with the policy described in the Instructions for Authors (www.plantphysiol.org) is: Michael A. Phillips (michael.phillips@cragenomica.es).

J.M.R. and J.G. designed the experiments; L.P.W., A.G., A.H., M.O., B.R., J.-P.S., and M.A.P. performed the experiments; L.P.W. and M.A.P. developed the methods; L.P.W., J.M.R., and M.A.P. analyzed the data; A.G. and J.-P.S. provided specialized technical knowledge; A.G., J.-P.S., and J.G. edited the manuscript; L.P.W. and M.A.P. wrote the article.

[C] Some figures in this article are displayed in color online but in black and white in the print edition.

[W] The online version of this article contains Web-only data.

[OPEN] Articles can be viewed online without a subscription.

www.plantphysiol.org/cgi/doi/10.1104/pp.114.245191

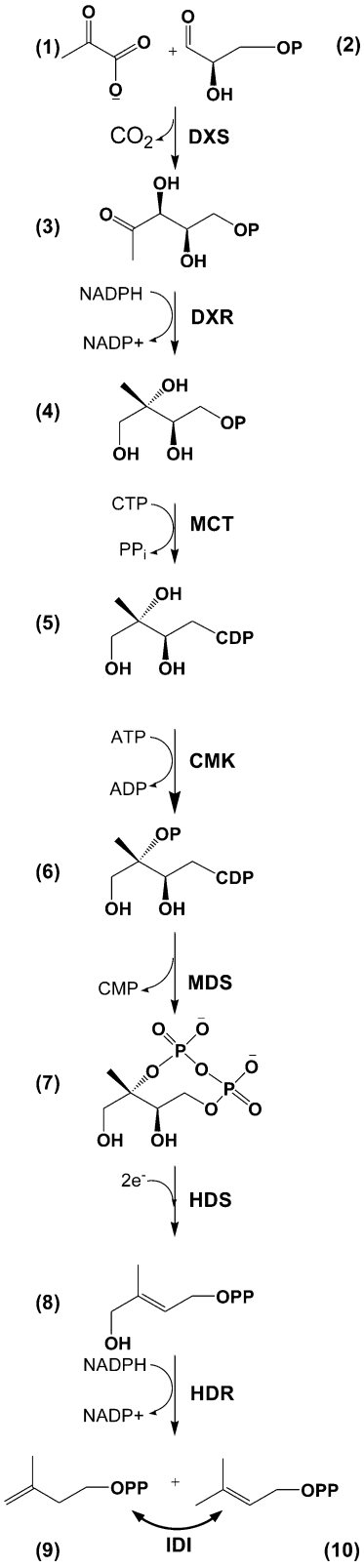

Figure 1. Scheme of the MEP pathway. Structures: (1) pyruvate, (2) D-glyceraldehyde 3-phosphate, (3) 1-deoxy-D-xylylose 5-phosphate, (4) MEP, (5) 4-(cytidine 5′diphospho)-2-*C*-methyl-D-erythritol (CDP-ME), (6) 2-phospho-4-(cytidine 5′diphospho)-2-*C*-methyl-D-erythritol (CDP-MEP), (7) 2-*C*-methyl-D-erythritol-2,4-cyclodiphosphate (MEcDP), (8) 1-hydroxy-2-methyl-2-(*E*)-butenyl 4-diphosphate (HMBDP), (9) IDP, and (10) DMADP. CMK, CDP-ME kinase; IDI, IDP isomerase; MCT, MEP cytidylyltransferase; MDS, MEcDP synthase; HDS, HMBDP synthase; HDR, HMBDP reductase; OP, monophosphate; OPP, pyrophosphate.

Posttranscriptional regulation was revealed by studies showing that the amount of enzyme catalyzing the first step, 1-deoxyxylulose 5-phosphate synthase (DXS), is upregulated in mutants blocked in later steps, even while the transcripts of all MEP pathway genes are down-regulated (Guevara-García et al., 2005). Up-regulation of DXS protein was also noted in an Arabidopsis mutant defective in the stromal Casein Lytic Proteinase (Clp) complex (Flores-Pérez et al., 2008). Further investigation implicated protease degradation in the plastid as a fundamental regulatory mechanism for the activity of both DXS and the enzyme catalyzing the subsequent step, 1-deoxyxylulose 5-phosphate reductase (DXR). A J-protein (J20) has been described that specifically directs misfolded DXS protein to the Heat Shock Protein70 chaperone for repair or to the Clp protease complex for degradation under heat stress (Pulido et al., 2013). Constitutive expression of either DXS (Estévez et al., 2001) or DXR (Carretero-Paulet et al., 2006) leads to higher levels of isoprenoid end products, such as chlorophylls, tocopherols, and carotenoids, in plate-grown Arabidopsis seedlings. Yet there are still many questions about the regulatory roles of DXS and DXR in the MEP pathway.

In addition to studies at the gene and protein levels, efforts to understand the metabolic control of the MEP pathway have also been undertaken by quantitative analysis of flux. These efforts initially focused on trees emitting isoprene, because this C_5 hemiterpenoid represents the bulk of MEP pathway flux in such species and is easily detected (Sharkey et al., 1991). Isoprene synthase generates isoprene from DMADP, which is maintained at constant levels relative to IDP by IDP isomerase (Ramos-Valdivia et al., 1997). Isoprene emissions correlate directly with DMADP concentrations (Brüggemann and Schnitzler, 2002; Magel et al., 2006), making isoprene measurements a useful probe for measuring flux in the MEP pathway.

In poplar (*Populus* spp.), oak (*Quercus* spp.), and aspen (*Populus* spp.), DMADP-derived isoprene emissions drop off quickly when the light is turned off in controlled gas exchange experiments (Li and Sharkey, 2013), underscoring the absolute requirement for photosynthetically derived ATP and NADPH in the MEP pathway of leaves. Li and Sharkey (2013) quantified nearly all pathway intermediates in aspen leaves under physiological conditions and noted that substrates of steps requiring reducing equivalents such as 2-C-methylerythritol-2,4-cyclodiphosphate (MEcDP) accumulated to high levels, whereas those of nonreducing steps were present at much lower concentrations. Using ^{31}P-NMR, MEcDP has also been observed to accumulate under high light intensities (Rivasseau et al., 2009) and in detached leaves

incubated with cadmium (Mongélard et al., 2011), a heavy metal that inhibits 1-hydroxy-2-C-methyl-2-(E)-butenyl-4-diphosphate (HMBDP) synthase (HDS; Fig. 1). MEcDP was recently proposed to have plastid-to-nucleus retrograde signaling activity, modulating nuclear gene expression and salicylic acid accumulation in response to stress (Xiao et al., 2012). This role suggests a mechanism that exports MEcDP out of the plastid. Another example of branching in the MEP pathway has also been noted. MEcDP is normally converted to HMBDP en route to IDP and DMADP production by HMBDP reductase (HDR) in the stroma. However, root wounding, oxidative stress, and nitrate deficiency in Arabidopsis leaves can trigger diversion of HMBDP into glycosylated hemiterpenoids (Ward et al., 2011).

In recent years, there has been increasing interest in manipulating the MEP pathway to increase the production of various isoprenoid end products. Kinetic models of metabolism that describe metabolic networks in terms of kinetic equations are useful in this regard (Rohwer, 2012). By assigning kinetic parameters to each reaction in the network, they enable the prediction of product formation for any concentration of enzyme or metabolic intermediate (Colón et al., 2010). Targets for pathway manipulation can be identified with metabolic control analysis (MCA), which involves the measurement of control coefficients (i.e. quantities that indicate the degree of control an individual enzyme exerts over the flux through a pathway or the steady-state concentration of a metabolic intermediate; Fell, 1992; Kacser and Burns, 1995). For metabolic networks for which only limited kinetic information is available, control coefficients can be calculated by manipulating enzyme activity and observing the effect of a fractional change in activity on the fractional change in flux or metabolite concentration. Flux through metabolic pathways with complicated stoichiometry or whose end products are themselves substrates for other metabolic pathways is most conveniently measured using a stable isotopic label such as ^{13}C. The incorporated isotopic label can then be analyzed by mass spectrometry or NMR. Examples of ^{13}C-based measurements of metabolic flux include heterotrophic (Williams et al., 2008; Alonso et al., 2010; Allen et al., 2012) and mixotrophic (Kempa et al., 2009) plant cell culture systems, photoautotrophic microbial systems (Shastri and Morgan, 2007; Young et al., 2011), individual leaves of whole plants (Hasunuma et al., 2010; Ghirardo et al., 2014), and whole Arabidopsis rosettes (Szecowka et al., 2013).

Here we describe the use of soil-grown whole plants to examine flux in the MEP pathway in Arabidopsis using a photoautotrophic $^{13}CO_2$ labeling method under controlled physiological conditions. This approach allowed us to measure in vivo flux of carbon under completely natural conditions in individual plants. Using this experimental system, we examined the quantitative flux control of DXS in the MEP pathway. A high flux control coefficient (FCC) value indicated that DXS is the major controlling enzyme in photosynthetically active leaf tissue. The whole-plant labeling approach also unexpectedly revealed a second pool of MEcDP sequestered from the MEP pathway that responds to changes in DXS activity. These findings have major implications for MEP pathway regulation and the engineering of isoprenoid biosynthesis in plants.

RESULTS

Whole-Plant Labeling with $^{13}CO_2$ under Physiological Conditions Maintains Steady-State Metabolite Concentrations

To investigate the metabolic flux through the MEP pathway under natural, physiological conditions, we used short-term $^{13}CO_2$ kinetic labeling of whole Arabidopsis plants at the rosette stage in an environmentally controlled dynamic flow cuvette. Prior to initiating labeling, gas exchange measurements with normal air (380 μL L^{-1} $^{12}CO_2$, including 1.1% $^{13}CO_2$) indicated that a photosynthetic steady state of about 4 μmol CO_2 m^{-2} leaf area s^{-1} was typically reached in 30 min at 140 photosynthetic photon flux density (PPFD). A step change to a labeling atmosphere (380 μL L^{-1} $^{13}CO_2$, 99.9%) was followed by 6 to 60 min of labeling, harvest, and analysis of ^{13}C-label incorporation into metabolites in plant extracts.

In order to verify that labeling did not alter metabolite pool sizes and confirm our assumption of a metabolic steady state, we measured absolute concentrations of the MEP pathway intermediates 1-deoxyxylulose 5-phosphate (DXP), MEcDP, and DMADP in wild-type plants after different lengths of time in a labeling atmosphere (Fig. 2). Our observations confirmed that the ^{13}C label was readily detectable at quantifiable levels even in our earliest time points but had no significant effect on metabolite pool sizes (*P* values for DXP, MEcDP, and DMADP were 0.67, 0.10, and 0.36, respectively) over the time course. Therefore, we consider kinetic inferences made under the assumption of steady-state conditions in these experiments to be justified.

$^{13}CO_2$ Administered in the Light Does Not Supply the Mevalonate Pathway

To ensure that the ^{13}C label in our DMADP pool could be attributed solely to flux through the MEP pathway, we attempted to measure ^{13}C flux through the mevalonate pathway after $^{13}CO_2$ labeling by analysis of mevalonate in labeled plant extracts. ^{13}C-labeled and unlabeled mevalonate standards were used to establish the separation and detection of this metabolite as a well-resolved peak at 6.1 min by liquid chromatography coupled to tandem mass spectrometry (LC-MS/MS) operating in multiple reaction monitoring (MRM) mode (Supplemental Fig. S1A). Unlabeled mevalonate was readily detected in plant extracts (Supplemental Fig. S1B). However, even after 45 min of labeling, none of the precursor/product ion scan combinations performed showed any ^{13}C incorporation. Taken together with the detection of ^{13}C in the MEP pathway intermediates in as little as 6 min, this result indicates that

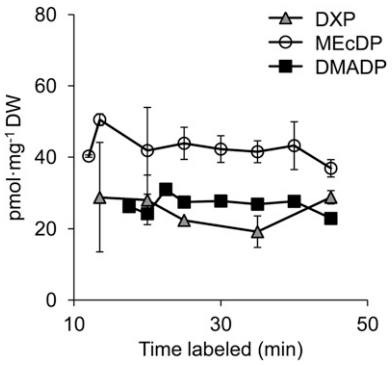

Figure 2. Levels of prominent MEP pathway metabolites in Arabidopsis rosettes during $^{13}CO_2$ labeling experiments. For DXP and MEcDP, absolute quantification was carried out by spiking plant extracts from various labeling times with unlabeled standard and by comparison of the relative peak size under the LC-MS/MS conditions described in the "Materials and Methods." For DMADP, quantification was based on the addition of unlabeled standard prior to acid hydrolysis to isoprene gas and headspace analysis by GC-MS. No statistically significant change in DXP ($P = 0.67$), MEcDP ($P = 0.10$), or DMADP ($P = 0.36$) was noted as a consequence of labeling with 380 μL L^{-1} $^{13}CO_2$. DW, Dry weight.

in illuminated, intact Arabidopsis plants, newly fixed carbon rapidly enters the plastidial MEP pathway but makes at most a negligible contribution to cytosolic isoprenoid formation via the mevalonate pathway.

$^{13}CO_2$ Is Rapidly Assimilated into MEP Pathway Intermediates

To confirm the source of carbon supplying the MEP pathway, we measured the incorporation of ^{13}C into several intermediates of the MEP pathway over time as a fraction of total carbon centers bearing a ^{13}C atom. When individual isotopologues of DXP were compared representing the $^{13}C_1$- through $^{13}C_5$-labeled species, the m_1 isotopologue was first to appear, followed by the successive appearance of m_2 and higher-labeled isotopologues up to m_5 (Fig. 3A). The abundance of m_1 ions declined quickly after peaking at approximately 8 min, followed by the decline of m_2 ions and so forth as higher-labeled m_4 and m_5 species overtook them in total abundance at later labeling points (>12 min). A similar labeling pattern was observed for MEcDP and DMADP (Fig. 3, C and E).

Using the full complement of m_1- through m_5-labeled DXP species from plants labeled for different lengths of time, we calculated the total fraction of labeled carbon in the DXP pool (Fig. 3B) as a function of time. This exponential curve showed the expected rise to maximum and approached a proportion of approximately 0.55 total DXP labeling for wild-type plants. The maximum labeling of MEcDP in wild-type plants approached a similar level (Fig. 3D). However, the maximal labeling observed in DMADP approached about one-half of this, peaking at a proportion of 0.28 at the longest labeling time points (Fig. 3F), most likely reflecting the presence of other sources of DMADP or other prenylated compounds, such as cytokinins, which release isoprene upon acid hydrolysis and so are measured as DMADP in our methods.

Steady-State Flux in the MEP Pathway Was Calculated from DXP Pool Size and ^{13}C Incorporation Rates

Kinetic data from DXP label incorporation experiments (Fig. 3B) were used to calculate rate constants for DXP turnover by fitting these data to the equation describing an exponential rise to maximum. Fluxes in the MEP pathway were obtained by multiplying this rate constant by the DXP pool size as judged by LC-MS/MS measurements. In addition to wild-type plants, we applied this approach to a suite of mutant and transgenic Arabidopsis lines presenting a range of DXS activities (Table I), based on a highly sensitive LC-MS/MS-based assay (Supplemental Fig. S2). A natural DXS mutant *dxs3* (Araki et al., 2000; renamed from *chill sensitive5*, in Phillips et al., 2008) and three 35S:DXS lines were included. The DXS activities of approximately 40 independent 35S:DXS lines were initially screened, and three single insert homozygous lines were selected for flux analysis that maintained stable and elevated DXS activities across multiple generations (Supplemental Fig. S3). Labeling experiments using 30 individual plants over a 60-min time series were used to calculate a flux of 3.44 ± 0.35 pmol mg^{-1} dry weight min^{-1} for wild-type plants, whereas the *dxs3* temperature-sensitive mutant line showed a decrease in flux to about 80% that of the wild type. On the other hand, the flux in 35S:DXS lines was almost twice that of the wild type.

The FCC for DXS Is High under Photosynthetic Steady-State Conditions

In a linear pathway, the FCC of an enzyme ranges from 0 to 1 and indicates the fractional change in flux in a pathway given a fractional change in that enzyme's activity. An FCC of 0 indicates that increasing that enzyme's activity will have no effect on flux, whereas an FCC of 1 means that a change in flux will be directly proportional to changes in enzyme activity (Fell, 1997). According to the mathematical framework of MCA (Fell, 1992; Rohwer, 2012), the FCC can be determined directly by correlating flux to different levels of enzyme activity. The flux values of the wild type and DXS mutant and transgenic lines were plotted as a function of their corresponding enzyme activities (Fig. 4), and the FCC of DXS was calculated from the slope of the linear regression of these data, scaled by the ratio of DXS activity to flux at the wild-type activity level (see the "Materials and Methods"). Based on this approach, we observed that under steady-state conditions in wild-type plants, the FCC of DXS was 0.82. The summation theorem of MCA states that the FCCs of all enzymes in a metabolic pathway sum to 1 (Fell, 1997). This suggests that during the day under normal light

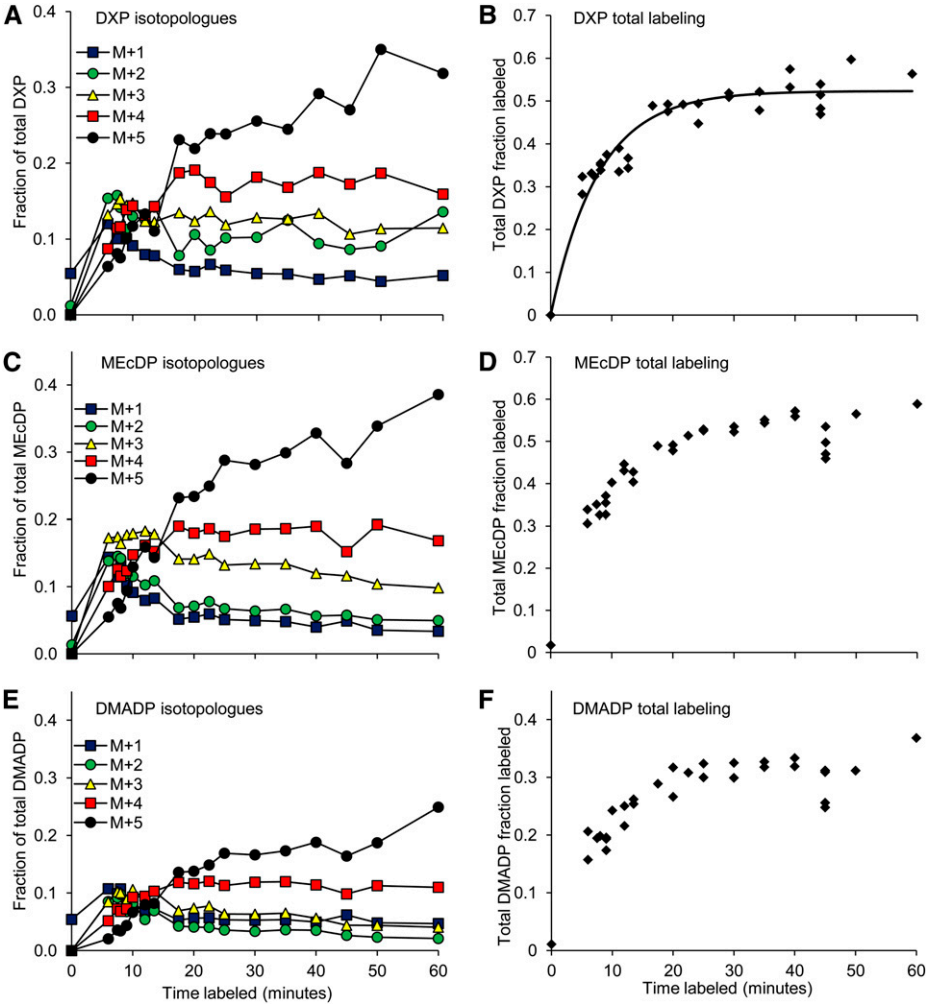

Figure 3. Time course of ^{13}C label incorporation into intermediates of the MEP pathway in wild-type Arabidopsis rosettes. Wild-type plants were labeled in vivo from 6 to 60 min in an atmosphere containing 380 μL L^{-1} $^{13}CO_2$ before being flash frozen and extracted. A and B, Using an LC-MS/MS triple quadrupole system, the relative abundance of DXP isotopologues representing the m_0 to m_5 ^{13}C labeled species was determined by MRM in negative mode of ions ranging from *m/z* 212.95 → 96.9 to *m/z* 217.95 → 96.9 in the DXP peak eluting at 8.0 min (m_0 ions not shown). Total DXP labeling was calculated from individual isotopologue abundances. C and D, The abundance of individual MEcDP isotopologues was similarly determined from MRM of ions ranging from *m/z* 276.96 → 78.9 to *m/z* 281.96 → 78.9 in the MEcDP peak eluting at 9.5 min in the same chromatographic separation. E and F, DMADP isotopologue abundances were determined after acid-catalyzed conversion to isoprene gas and GC-MS analysis. Positive chemical ionization using methane as the reagent gas was employed to minimize rearrangement of the molecular ion, simplifying label incorporation calculations. Corrections for hydride abstraction and charge exchange of isoprene during ionization are described in the Supplemental Methods S1. Fluxes through the MEP pathway in diverse lines were measured by curve fitting the exponential rise to maximum in DXP labeling (the wild type is shown) to calculate kinetic rate constants as described in the "Materials and Methods." Plateau labeling for MEcDP and DMADP was estimated from averaging the latter times points because the incorporation of label in downstream metabolites could not be modeled as an exponential rise to maximum. [See online article for color version of this figure.]

conditions, DXS is the major flux-controlling enzyme of the MEP pathway.

The Concentration Control Coefficients of DXS for Plastid DXP, MEcDP, and DMADP Are High under Normal Light Conditions

A concentration control coefficient (CCC) can be calculated in analogy to an FCC, indicating the fractional change in the concentration of a metabolite given a fractional change in enzyme activity. However, CCCs can be either positive or negative and significantly larger in magnitude than FCCs (Fell, 2005). The plastidic pool sizes of MEcDP and DMADP were calculated from total pool sizes (Fig. 5) by assuming that all DXP is associated with the MEP pathway and biosynthesized in the plastid (Tambasco-Studart et al., 2005). The chloroplast fractions of the later intermediates MEcDP and DMADP, subject

Table I. *Flux in the MEP pathway of DXS transgenic and mutant lines*

The total labeled fraction of DXP at various labeling times (Fig. 4B) was plotted versus labeling time and the data fitted to an equation describing exponential rise to maximum ($A \times [1 - e^{[-k \times t]}]$), where A is the maximum labeling plateau, *t* is the labeling time, and *k* is the kinetic rate constant. Details are provided in the "Materials and Methods." Flux was calculated by multiplying DXP pool size (obtained from LC-MS/MS measurements) by the fitted rate constant *k*.

Plant Line	A	DXP Pool Size	*k*	Flux
		pmol mg^{-1} dry wt	*min^{-1}*	*pmol mg^{-1} dry wt min^{-1}*
dxs3	0.588 ± 0.02	23.1 ± 1.24	0.117	2.72 ± 0.15
Wild type	0.523 ± 0.01	26.9 ± 1.91	0.128	3.44 ± 0.24
DXS12	0.505 ± 0.02	34.3 ± 1.53	0.135	4.64 ± 0.21
DXS16	0.479 ± 0.01	34.3 ± 1.47	0.181	6.20 ± 0.27
DXS24	0.465 ± 0.01	34.5 ± 2.55	0.193	6.68 ± 0.49
DXS45	0.466 ± 0.01	35.2 ± 1.45	0.181	6.36 ± 0.26

to possible export, were then calculated by normalizing their steady-state ^{13}C incorporation levels to that of DXP (Fig. 6). For each of the intermediates, the dependence of its chloroplast pool size on DXS activity was then described with a linear regression (Fig. 7), and the slope was used to calculate the respective CCC. DXS exerted substantial positive control on the levels of all intermediates, but the CCC for MEcDP (0.74) was considerably higher than those for DXP (0.35) or DMADP (0.34).

In turn, we investigated the effect of DMADP concentration on DXS activity because DMADP (and IDP) have been shown to regulate DXS activity in poplar through negative feedback inhibition (Banerjee et al., 2013; Ghirardo et al., 2014). Various concentrations of DMADP were added to wild-type Arabidopsis protein extracts and the effect on DXS activity was measured (Supplemental Fig. S4) in order to calculate the elasticity of DXS for DMADP, defined as the fractional change in enzyme velocity given a fractional change in metabolite concentration. The near-zero value obtained (−0.069) indicates that under physiological concentrations of substrates and effectors, DMADP has a very minor effect on DXS activity in Arabidopsis. The response of flux to an external metabolite (response coefficient) may be calculated by taking the product of the elasticity and FCCs of the affected enzyme (Fell, 1997). Using the above data, we calculate a response coefficient of −0.057 for the effect of DMADP on DXS. These data indicate that DMADP inhibition does not play a major role in regulating flux through the MEP pathway in Arabidopsis under normal growth conditions.

Overexpression of DXS Has Minimal Effects on Transcript Levels of Other MEP Pathway Genes

DXS transcript levels were measured in DXS mutant and transgenic lines and compared with those of wild-type plants by quantitative real-time PCR. We also examined the expression of downstream genes of the MEP pathway in the same lines to determine whether altering DXS expression would have any effect on their transcript abundance. The expression of MEP pathway genes is known to follow a diurnal rhythm in plants (Dudareva et al., 2005; Loivamäki et al., 2007; Covington et al., 2008), and values reported here represent midday transcript levels that should be at or near their maximum levels. In the temperature-sensitive DXS mutant *dxs3*, there was a notable down-regulation of all MEP pathway genes including *DXS* to about one-half that of the wild type. Meanwhile, in transgenic, overexpressing 35S:DXS plants, the transcripts for *DXS* were higher than in wild-type plants as expected (Fig. 8), reaching levels between 2 and 4 times higher than the peak expression levels of wild-type plants at midday. However, the expression of other MEP pathway genes downstream from *DXS* was not altered in the 35S:DXS plants except in one line (*DXS24*). This result indicates that manipulation of *DXS* expression generally does not affect the expression of other pathway genes. We also observed a lack of direct correspondence between *DXS* transcript levels and DXS activity in planta (Fig. 8; Supplemental Fig. S3).

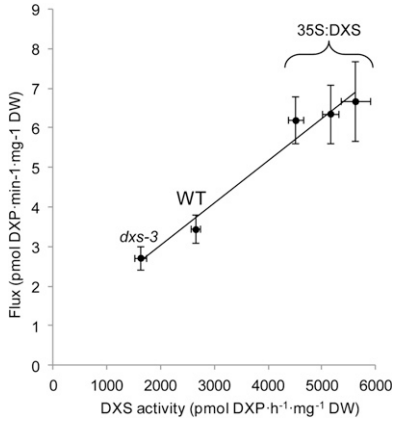

Figure 4. Flux control of DXS. The graph shows that the flux through the MEP pathway is a direct function of DXS activity. Fluxes are plotted for the DXS mutant (*dxs3*), 35S:DXS transgenic lines, and the wild type. Error bars indicate SES of both the flux (vertical) and DXS activity (horizontal) values. The line is a linear regression of the data with equation $y = 0.0011x + 0.8961$ ($R^2 = 0.973$).The FCC was calculated from the slope of this regression, yielding a value of 0.82 for DXS. DW, Dry weight; WT, wild type.

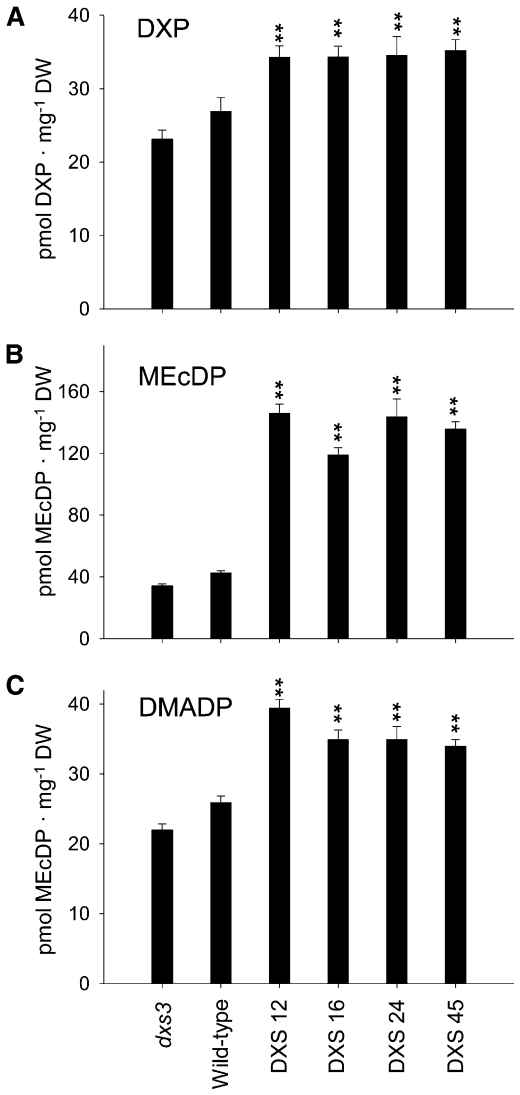

Figure 5. Pool sizes of DXP, MEcDP, and DMADP in wild-type, DXS mutant (*dxs3*), and DXS-overexpressing (DXS12, DXS16, DXS24, and DXS45) transgenic lines. A and B, Absolute concentrations of DXP (A) and MEcDP (B) were normalized to added unlabeled standard and compared with an external standard curve. C, DMADP was quantified by GC-MS after acid-catalyzed hydrolysis to isoprene gas and normalized to added unlabeled standard. Each metabolite concentration was determined using at least 10 individual plants. Error bars indicate SE. Double asterisks indicate significance at $P < 0.01$ (Student's *t* test). DW, Dry weight.

Total ^{13}C Label Incorporation into MEP Pathway Intermediates Reveals DXS-Mediated Control over a Second Pool of MEcDP Outside the Plastid

When we compared the labeling plateaus of the MEP pathway intermediates DXP, MEcDP, and DMADP among our altered *DXS* and wild-type lines, DXP in wild-type plants had a maximum labeling fraction of approximately 0.55 relative to total pool size (Fig. 6A). The *dxs3* mutant line showed a slightly higher average level of maximal incorporation and the 35S:DXS lines slightly lower levels (Fig. 6A), but overall no significant change in maximal DXP labeling was observed across a range of DXS activities. Likewise, no significant differences in DMADP maxima were noted among wild-type, *dxs3*, or transformed lines, although the maximal labeling proportion (0.30) was about one-half as much as DXP (Fig. 6C). However, in the case of MEcDP, ^{13}C label incorporation in the DXS-overexpressing lines was significantly lower than in the wild-type or *dxs3* mutant, with a proportion of about 0.30 compared with 0.60 in wild-type or *dxs3* plants (Fig. 6B).

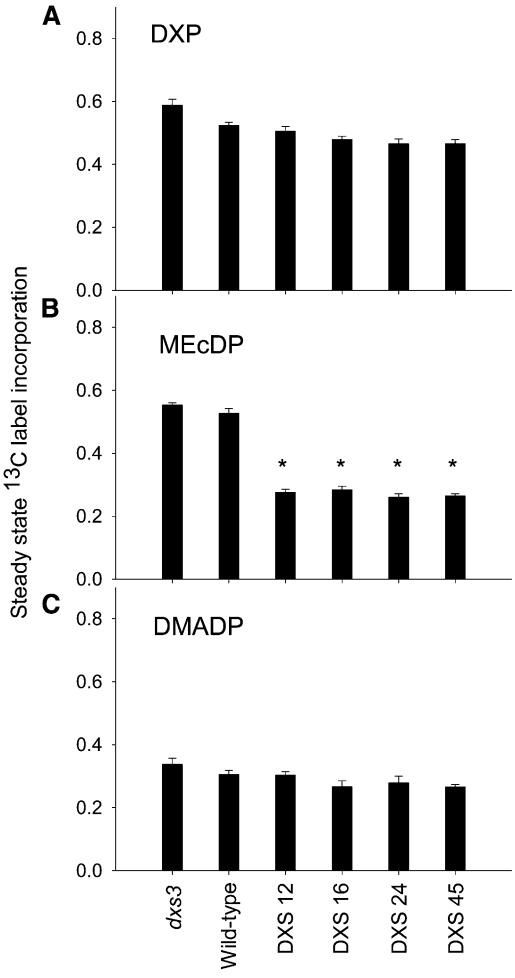

Figure 6. Incorporation of the $^{13}CO_2$ label into the MEP pathway intermediates DXP, MEcDP, and DMADP in wild-type, DXS-overexpressing (DXS12, DXS16, DXS24, and DXS45), and DXS mutant (*dxs3*) lines. A, Steady-state labeling of DXP was determined by fitting time course labeling data to an exponential curve ($A \times [1 - e^{[-k \times t]}]$), where A is the labeling plateau, *t* is the labeling time, and *k* is the kinetic rate constant based on total DXP labeling in plants subjected to a $^{13}CO_2$ labeling atmosphere from 6 to 60 min. B and C, Steady-state labeling of MEcDP (B) and DMADP (C) was determined by averaging the last four points of the time course (40, 45, 50, or 60 min). The asterisk indicates a significant decrease compared with the wild type based on a Student's *t* test with $P < 10^{-6}$. Error bars indicate the SE.

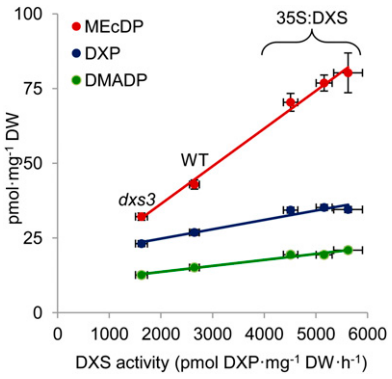

Figure 7. Concentration control of DXS on MEP pathway intermediates. The graph shows the plastidic pool sizes of MEcDP, DXP, and DMADP as a function of DXS activity for DXS mutants (*dxs3*), 35S:DXS transgenic lines, and the wild type. Error bars indicate SES of pool sizes (vertical) as well as DXS activity values (horizontal). Plastid pool sizes of MEcDP and DMADP associated with the MEP pathway were calculated by assuming that DXP is only biosynthesized through the plastid MEP pathway and normalizing the steady-state fraction of ^{13}C incorporated into MEcDP and DMADP to that incorporated into DXP, as described in the main text. The lines are linear regressions of the data with the following equations: MEcDP, $y = 0.0126x + 11.157$ ($R^2 = 0.994$); DXP, $y = 0.0031x + 18.561$ ($R^2 = 0.951$); and DMADP, $y = 0.002x + 9.6238$ ($R^2 = 0.979$). Control coefficients were calculated from the slope of these regressions yielding values of 0.35, 0.74, and 0.34 for DXP, MEcDP, and DMADP, respectively. DW, Dry weight; WT, wild type. [See online article for color version of this figure.]

Absolute pool sizes of each metabolite were also compared between lines (Fig. 5). DXP and MEcDP were quantified in liquid extracts of wild-type, *dxs3* mutant, and 35S:DXS lines by LC-MS/MS, whereas DMADP quantification was performed after acidolysis to isoprene gas. The 35S:DXS lines showed a significant elevation of DXP pool size, from 26 pmol mg^{-1} dry weight in the wild type to approximately 34 pmol mg^{-1} dry weight for all 35S:DXS lines ($P < 0.0001$), whereas the *dxs3* mutant had DXP levels at about 85% that of the wild type (23 pmol mg^{-1} dry weight; $P = 0.10$). In the case of MEcDP, however, absolute concentrations rose about 3 times in the 35S:DXS lines (to 120–145 pmol mg^{-1} dry weight from the wild-type level of 42 pmol mg^{-1} dry weight). For DMADP, the increases in concentration mirrored those of DXP, reaching a maximal 1.5-fold increase ($P < 10^{-8}$) among 35S:DXS lines (39 pmol mg^{-1} dry weight) compared with wild-type levels (25 pmol mg^{-1} dry weight).

The 3-fold increase in MEcDP pool size when DXS was upregulated (Fig. 5B) was very conspicuous in light of the drop in plateau labeling levels of MEcDP in these same lines (Fig. 6B). This observation could be explained by the existence of a second pool of MEcDP metabolically isolated from the MEP pathway and the Calvin-Benson-Bassham (CBB) cycle. To explore this possibility, we measured end-of-night MEcDP concentrations in the wild type and in a 35S:DXS line just before the onset of dawn. MEcDP concentrations in spinach (*Spinacia oleracea*) and poplar were previously shown to rapidly decline in the darkness due to turnover of the plastid-localized pool (Rivasseau et al., 2009; Li and Sharkey, 2013). When we compared predawn MEcDP concentrations, 35S:DXS plants had nearly 5-fold more MEcDP (111.3 ± 9.91 pmol mg^{-1} dry weight) than wild-type plants (23.23 ± 1.01 pmol mg^{-1} dry weight). The size of this end-of-night pool in transgenic lines roughly matches the unlabeled pool size inferred from photosynthetic steady-state labeling data. This second, persistent pool of MEcDP could also be detected by placing plants in complete darkness for 30 min during the middle of a 10-h light period. In 35S:DXS lines, 78% of the MEcDP measured in the light remained after dark treatment, whereas MEcDP dropped to 48% after the same treatment for wild-type plants (Fig. 9). By contrast, the drop in DXP levels for 35S:DXS plants was nearly identical to that of wild-type plants (47% and 45% remaining, respectively). This latter observation agrees with our assumption of a single DXP pool in calculating the plastid-cytosol partitioning of DMADP and MEcDP (Fig. 7).

The calculation of extraplastidic MEcDP based on these assumptions indicated that all MEcDP was associated with the chloroplast-localized MEP pathway for the wild type and the *dxs3* mutant line, but not for the DXS-overexpressing lines (Fig. 10). However, both pools were affected by DXS activity. The estimated chloroplast MEcDP levels showed a linear increase with increasing DXS activity, ranging from 32 to 80 pmol mg^{-1} dry weight, and the MEcDP pool external to the MEP pathway in the 35S:DXS lines also showed a linear increase with DXS activity. If MEcDP efflux represents a natural process, a sensitivity to increases in DXS might be expected considering the high FCC we measured for this enzyme.

DXS Overexpression Results in Only Slightly Higher Accumulation of Isoprenoid End Products

In order to determine the effect of altered DXS activity on isoprenoid end products, the levels of chlorophylls and major carotenoids were analyzed by HPLC with diode array detection. Overexpression of DXS was previously linked to increases in isoprenoid end products such as photosynthetic pigments and α-tocopherol in Arabidopsis plate-grown seedlings (Estévez et al., 2001; Carretero-Paulet et al., 2006), but such studies had not been conducted on fully grown plants raised under realistic physiological conditions. We detected modest increases in end product accumulation of some but not all transformed lines overexpressing DXS (Fig. 11). Compared with wild-type plants, the *dxs3* mutant line with decreased DXS activity had slightly lower levels of chlorophylls and carotenoids with decreases in the range of 5% to 12% relative to the wild type. In the DXS-overexpressing lines, increases on the order of 5% to 15% were noted for many of the chlorophylls and major carotenoids compared with wild-type plants.

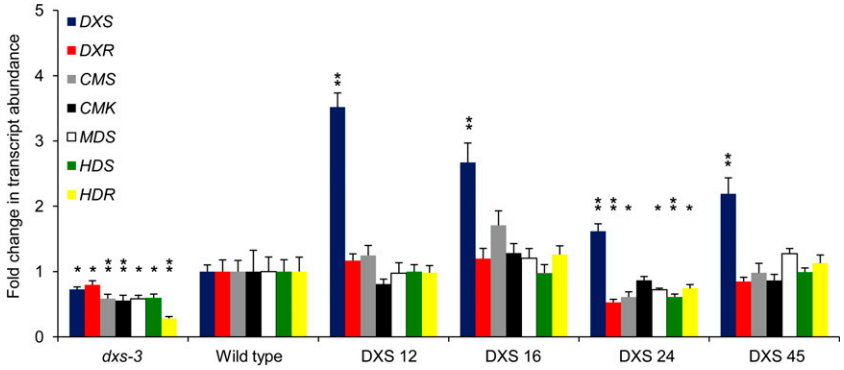

Figure 8. Transcript levels of MEP pathway genes at midday in transgenic (DXS12, DXS16, DXS24, and DXS45) and mutant (*dxs3*) lines with altered DXS activity and in wild-type controls. Relative quantification was performed according to the efficiency corrected model (Pfaffl, 2001). Efficiencies were obtained from the slope of dilution curves using control cDNA diluted from 1 to 1024 times at 4× intervals. Fold change values for each gene were calculated by comparison with the expression of the same gene in wild-type plants (control). Target gene expression was normalized to the RP2ls (At4g35800) and APT1 (At1g27450) genes weighted equally. Error bars indicate the SE of four biological replicates ($n = 4$) analyzed in triplicate SYBR green assays. Single asterisks indicate significant change relative to the wild type using a paired *t* test with a cutoff of $P = 0.05$. Double asterisks indicate a significant difference from the wild type using the same test with a cutoff of $P = 0.01$. For abbreviations of DXS pathway genes, see Figure 1. [See online article for color version of this figure.]

DXS Has a Positive Feedback Effect on the Carbon Dioxide Assimilation Rate

The general increase in photosynthetic pigments observed with an increase in DXS activity correlated to an increase in the overall rate of net carbon dioxide (CO_2) assimilation. There was a significant correlation (R^2 = 0.97) between the CO_2 assimilation rate and DXS activity for wild-type, mutant, and overexpressing lines, including a decrease in overall rate for the *dxs3* mutant and a proportional increase in assimilation rates for 35S:DXS lines with higher DXS activities (Fig. 12). Although the correlation was highly significant, the photosynthetic response factor to increasing DXS activity was low, yielding a maximum net increase of about 10% in total carbon assimilation even when DXS activity was more than 2-fold above wild-type levels. The magnitude of the increase was very similar to that observed among chlorophylls and carotenoids due to increased DXS levels.

DISCUSSION

Newly Assimilated Carbon Supplies the Plastidial Isoprenoid Pathway in Arabidopsis Leaves

Whole-plant kinetic labeling assays were used to probe the flux of carbon into the MEP pathway in actively photosynthesizing, fully grown, rosette stage Arabidopsis plants. Under illumination, newly fixed CO_2 is rapidly assimilated into glyceraldehyde-3-phosphate (G3P) and other metabolite pools of the CBB cycle. G3P can in principle be converted into pyruvate through glycolytic reactions, providing both substrates of the MEP pathway to the chloroplast (Joyard et al., 2010; Szecowka et al., 2013), and Rubisco produces a small amount of pyruvate directly in the plastid through β-elimination of an enzyme-bound intermediate (Andrews and Kane, 1991). However, it is generally assumed that pyruvate must be imported from the cytosol as phosphoenolpyruvate (PEP; Sharkey and Monson, 2014) because neither phosphoglycerate mutase (Stitt and Ap Rees, 1979) nor enolase (Prabhakar et al., 2009) is expressed in the chloroplasts of mesophyll cells. Therefore, some steps leading to pyruvate formation may occur in the cytosol in adult rosette tissue and rely on export and reimport of phosphorylated metabolites via the triose phosphate and PEP transporters in Arabidopsis (Knappe et al., 2003). Labeling studies in poplar (Trowbridge et al., 2012), isotopic abundance analysis in other isoprene-emitting species (Affek and Yakir, 2003) and functional analysis of the PEP transporter

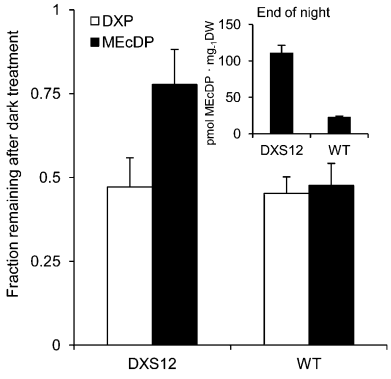

Figure 9. Effect of dark adaptation on concentrations of DXP and MEcDP in Arabidopsis leaves. Three wild-type or transgenic plants were placed in total darkness for 30 min at the midpoint of an 8-h day and then harvested ($n = 3$) for LC-MS/MS analysis. Means and SES of pool sizes relative to control plants left in the light are shown. Inset, Absolute MEcDP concentrations in wild-type and transgenic plants before dawn after a 16-h night ($n = 3$). Error bars show the SE. DW, Dry weight; WT, wild type.

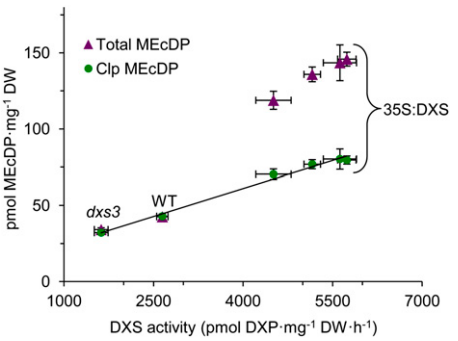

Figure 10. Total and chloroplast MEcDP levels as a function of DXS activity. Total MEcDP levels were determined as described in Figure 7. Based on the maximum label incorporation for the first MEP pathway intermediate (DXP), these values were extrapolated to calculate the chloroplast fraction of MEcDP. The line represents the linear regression of the chloroplast fraction with the equation $y = 0.0147x + 11.1566$ ($R^2 = 0.993$). DW, Dry weight; WT, wild-type DXS level. [See online article for color version of this figure.]

in the Arabidopsis *chlorophyl a/b binding protein underexpressed1* mutant (Voll et al., 2003) also support a cytosolic origin of plastidic pyruvate via PEP. Direct importation of pyruvate into the plastid by a sodium symporter to supply precursors to the MEP pathway has also been proposed (Furumoto et al., 2011), but expression of this gene in mature leaves may be too low to sustain the supply needed for plastid isoprenoid biosynthesis.

Our data support newly fixed carbon derived from CBB cycle reactions in the light as the principal source of substrate for the MEP pathway. This conclusion is consistent with the previously reported light-dependent nature of this pathway (Li and Sharkey, 2013). The successive appearance of m_1- through m_5-labeled isotopologues of DXP, MEcDP, and DMADP at regularly spaced intervals over a 1-h time course (Fig. 3) suggests that a pool undergoing rapid replenishment from atmospheric CO_2 can provide both substrates to the MEP pathway, although reimportation of PEP into the chloroplast may be accompanied by a significant dilution of label. At the same time, we failed to detect a ^{13}C label in the mevalonate pool of plants subjected to 45 min of labeling, suggesting that in the light under the growth conditions employed, flux through this pathway is minimal or fed from a separate carbon source. Thus, the labeling technique applied in this study labels the MEP pathway but not the mevalonate pathway.

DXP labeling reached a steady state after 30 min, but the fraction of the DXP pool labeled did not surpass 0.60 even after a full hour of labeling. This indicated that ambient CO_2 recently fixed through photosynthesis was not the only source of carbon entering the MEP pathway. The unlabeled fraction may originate from imported PEP (itself derived from previously fixed carbon sources such as transported sugars in the xylem [Kreuzwieser et al., 2002] and remobilized starch [Schnitzler et al., 2004]), and refixation of CO_2 evolved from mitochondrial and photorespiration (Ghirardo et al., 2011; Szecowka et al., 2013). The maximum proportion of labeling varied insignificantly under different levels of DXS activity, from which we conclude that the carbon source supplying the MEP pathway does not change when DXS activity is altered. The high proportion of m_4- and m_5-labeled DXP species observed at longer labeling times likely reflects the combined contribution of reimport of labeled PEP and low levels of pyruvate supplied directly by Rubisco β-elimination.

The High FCC of DXS Indicates Its Role in Controlling the MEP Pathway

The FCC is defined as the fractional change in steady-state flux given a fractional change in enzyme activity. Its value quantitatively describes the degree of control exerted by that enzyme over the flux through a pathway under a specific set of conditions and ranges from 0 to 1 in a linear pathway so that all FCCs add up to 1. We determined the FCC of DXS by measuring enzyme activity in wild-type plants compared with mutant and transgenic plants with altered DXS levels and by comparing these data to flux measurements of DXP in these same lines. All measurements were done on fully photoautotrophic plants under physiologically realistic growth conditions. The FCC obtained from such measurements is sensitive to the method used to fit the data to a function and may involve a complex polynomial or fitting to a perturbed state by way of a calculated deviation index (Small and Kacser, 1993). If deviation indices are calculated from these data (Supplemental Table S1), the FCC estimated by averaging deviations from a natural *DXS* mutant and overexpression lines is 0.84. However, we took advantage of the high degree of linearity over this range ($R^2 = 0.973$) and used linear regression to calculate the slope at the wild-type level using these same lines. The value obtained (0.82; Fig. 4) is consistent with the value obtained with the method of Small and Kacser (1993) and is consistent with earlier observations that up-regulation of the *DXS* gene correlates with higher accumulations of isoprenoid end products (Estévez et al., 2001; Carretero-Paulet et al., 2006). However, until now, the degree of control exerted by DXS over this pathway has not been quantitatively assessed. To our knowledge, this is the first time an FCC has been measured for an enzyme of the plant MEP pathway.

Despite the high FCC measured for DXS, its up-regulation in stably transformed lines did not result in the expected increases in isoprenoid end products. Although DXS activity was increased more than 2-fold, we noted only sporadic increases in chlorophylls and carotenoids formed by the MEP pathway. One explanation for the lower-than-expected increases in end product accumulation may lie with negative feedback inhibition of DXS by IDP and DMADP (Banerjee et al., 2013; Ghirardo et al., 2014), which allosterically bind to the thiamine diphosphate cofactor binding site as noncompetitive inhibitors. An increase in IDP and DMADP in vivo would then inhibit DXS activity, ultimately limiting the potential gains in flux expected by up-regulation of DXS. We tested this possibility in Arabidopsis by measuring the elasticity of

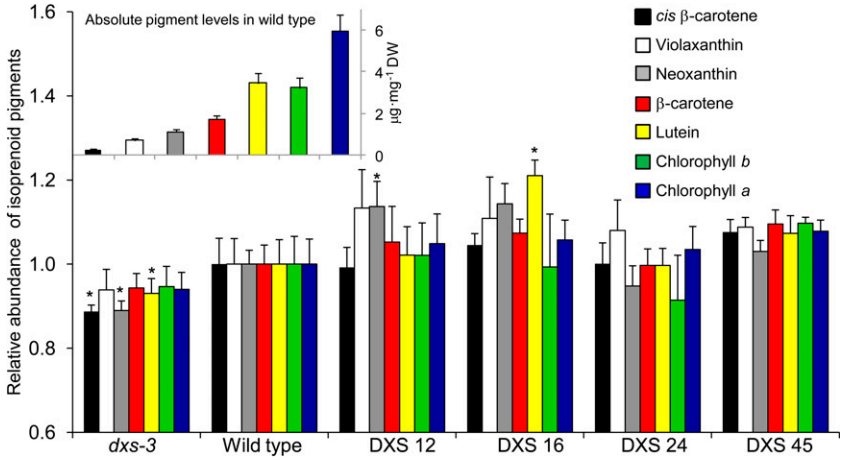

Figure 11. Accumulation of carotenoids and chlorophylls as representative isoprenoid end products in wild-type, DXS mutant, and DXS-overexpressing lines. Lines DXS12, DXS16, DXS24, and DXS45 express the full-length cDNA of the native DXS gene under the control of the 35S promoter. *dxs3* is a natural mutant of DXS (Araki, et al., 2000). Plants were harvested after 55 to 60 d of growth under short-day conditions but before the initiation of flowering. Four individual plants were used to characterize each line and means ± SES ($n = 4$) are shown. Inset, The absolute values of these compounds in wild-type plants are as follows: black, cis-β-carotene 0.24 μg mg dry weight ± 0.04; white, violaxanthin, 0.69 μg mg dry weight ± 0.16; gray, neoxanthin, 1.12 μg mg dry weight ± 0.17; red, β-carotene, 1.71 μg mg dry weight ± 0.27; yellow, lutein, 3.46 μg mg dry weight ± 0.54; green, chlorophyll *b*, 3.24 μg mg dry weight ± 0.66; and blue, chlorophyll *a*, 5.96 μg mg dry weight ± 1.05. The asterisk indicates a significant difference from wild-type values based on a Student's *t* test at $P < 0.05$. DW, Dry weight. [See online article for color version of this figure.]

DXS for DMADP, a quantity that indicates the fractional change in enzyme activity given a fractional change in metabolite concentration (Fell, 1997). Feedback inhibition is characterized by a large, negative elasticity for the inhibitory metabolite. However, the elasticity we observed in Arabidopsis, while negative, was small (−0.069), suggesting that feedback inhibition does not play a major role in regulating flux in this species under normal growth conditions. Although substantial DMADP-mediated inhibition of DXS does not occur in Arabidopsis, this does not exclude the feedback regulation of the MEP pathway under other physiological conditions. Generally, feedback inhibition may be more prominent in isoprene-emitting species such as poplar, which maintain much higher DMADP concentrations than Arabidopsis (Ghirardo et al., 2014). Another explanation for the lower-than-expected increases in stable isoprenoid end products may be due to diversion of flux into a separate pool of MEcDP when DXS is upregulated. Our calculations of MEcDP partitioning between the plastid and nonplastid pools indicate that this diversion occurs in DXS-overexpressing plants, but not in wild-type plants under our growing conditions. DXS overexpression may inadvertently trigger a natural efflux process involved in stress signaling that occurs under certain environmental conditions (Xiao et al., 2012; Zhou et al., 2012).

Cytosolic and Plastidic Pool Size Analysis Shows That Most of the Cellular DMADP Is in the Plastid

We took advantage of our steady-state labeling data and the assumption that all DXP is present in the plastid to estimate absolute sizes of chloroplast pools of MEcDP and DMADP. Curve-fitting calculations showed that the maximal ^{13}C labeling of DXP peaked at a fraction of 0.6 in time course experiments with wild-type plants (Fig. 6A). Using the maximal labeling of DXP to calculate the size of the plastid-localized DMADP pool, we estimate that 58% of cellular DMADP is in the chloroplasts, although maximal labeling of DMADP was only about

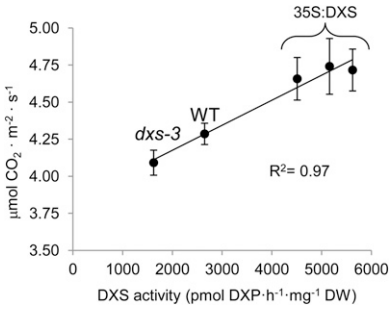

Figure 12. Effect of DXS activity on the net carbon assimilation rate. Net carbon assimilation was normalized to photosynthetically active (projected) leaf surface area as determined by photography of the rosette with size standards. Individual plants were acclimated for a minimum of 30 min or until photosynthesis had reached a steady state. Photosynthetic rates were estimated from the last minute of gas exchange measurements prior to the initiation of labeling by switching to an atmosphere containing $^{13}CO_2$. DXS activities were later determined using protein extracts from the same plants (Supplemental Fig. S2). The line represents the linear regression between photosynthetic rate and DXS activity with the equation $y = 0.00017x + 3.8379$ ($R^2 = 0.971$). DW, Dry weight; WT, wild type.

one-half that of DXP. This calculation is in agreement with previous literature reports (Nogués et al., 2006). Weise et al. (2013) recently showed that the detection of DMADP as isoprene after acid hydrolysis as used in this study overestimates the true amount of DMADP, most probably due to an additional unknown source of isoprene during acid hydrolysis. We can therefore assume that the fraction of DMADP that actually occurs in the chloroplast in Arabidopsis leaves is likely much higher than 58%. In any event, under illumination, the majority of total DMADP is present in the plastid and is turned over on a short (<10 min) time scale. The remainder is likely derived from prenylated compounds other than DMADP as well as a small pool of DMADP derived from the mevalonate pathway in the cytosol or other extraplastidic compartments. Although the extraplastidic pool of DMADP cannot be quantified reliably with the acid hydrolysis method, it nonetheless did not show significant turnover with newly fixed photosynthate based on the lack of ^{13}C label detected in mevalonate pools (Supplemental Fig. S1).

The Second Pool of MEcDP May Also Be Present in Wild-Type Plants

In plants overexpressing DXS, there was a 3-fold increase in the total amount of MEcDP (Fig. 5B), but the level of labeling from $^{13}CO_2$ was only one-half that seen in wild-type plants (Fig. 6B). These data pointed to a second pool of MEcDP, which is supported by the persistence of this intermediate in DXS-overexpressing plants after dark adaptation (Fig. 9) and at the end of the night. This second pool is not located in the chloroplast based on normalization of the MEcDP steady-state ^{13}C incorporation level to that of DXP (Fig. 10), and is not amenable to $^{13}CO_2$ labeling on a time scale of up to 1 h. However, both pools of MEcDP were highly sensitive to elevated DXS activity. By contrast, all of the MEcDP was associated with the MEP pathway in plastids in wild-type plants and plants with reduced DXS activity.

Although the second pool of MEcDP was not seen in wild-type plants under the growth conditions used in our study, we suggest that diversion of MEcDP from the MEP pathway may occur naturally under stress regimes that cause MEcDP to accumulate, either by increasing the level of DXS activity or decreasing the activity of later pathway steps. MEcDP efflux was recently described for an *Escherichia coli* strain overexpressing DXS (Zhou et al., 2012), possibly as a response to oxidative stress. MEcDP diversion may also result from pathogen attack as part of a stress response mediated by salicylic acid (Gil et al., 2005). This is consistent with participation of MEcDP in plastid-to-nucleus stress signaling (Xiao et al., 2012) and may depend on MEP pathway flux under different environmental conditions. Although the most likely location of MEcDP exported from the plastid is the cytosol, additional research is required to confirm its precise location and mode of action.

These findings help open new frontiers for both basic and applied research on the MEP pathway. Calculation of the FCC for DXS affirms its role as a major controlling step of isoprenoid formation in plants. However, the influence of DXS may be attenuated by efflux of MEcDP into a separate compartment. It is important to learn whether rising MEcDP levels signal any broader changes in the physiology of the plant in addition to those previously described (Xiao et al., 2012). Knowledge of the metabolic fate of the diverted MEcDP would also help clarify how the MEP pathway is regulated. From a metabolic engineering perspective, MEcDP diversion could decrease flux to a wide range of biotechnologically valuable products (Bouvier et al., 2005). Thus, identification of the regulatory network induced by high levels of MEcDP or any specific proteins responsible for MEcDP efflux would provide targets for disrupting this control mechanism that could allow researchers to increase flux to the MEP pathway end products IDP and DMADP. Such efforts would provide additional substrate for a wide range of isoprenoid end products, including photosynthetic pigments, plastoquinones, carotenoids, and diverse monoterpenes and diterpenes of pharmacological, agricultural, and industrial importance (Lange and Ahkami, 2013).

MATERIALS AND METHODS

Plant Lines and Growth Conditions

All experiments were carried out with individual Arabidopsis (*Arabidopsis thaliana*) ecotype Columbia 0 wild-type plants, transgenic lines generated from the same seed stocks, or the *dxs3* mutant, a naturally occurring temperature-sensitive mutant with reduced DXS activity (Araki et al., 2000; originally designated *chs5* by Phillips et al., 2008). Plants were grown in soil pots (7 × 7 × 8 cm) after storage for 3 d at 4°C in complete darkness. The pots were transferred to a growth chamber and grown under short-day (10-h-day/14-h-night) conditions at 21°C and 140 μmol m^{-2} s^{-1} PPFD for 1 month prior to use in labeling experiments. Transgenic lines were generated by vacuum infiltration of flowering-stage plants using *Agrobacterium tumefaciens* strain GV3101 harboring the pB7FWG2 plasmid (Karimi et al., 2002). The full-length coding sequence of Arabidopsis *DXS* was cloned in frame with a C-terminal enhanced GFP tag under control of the 35S promoter using entry vector pDONR207 and BP and LR clonase II kits (Invitrogen Technologies). *A. tumefaciens* cultures were grown overnight at 28°C in yeast extract and peptone medium containing rifampicin (150 μg mL^{-1}), gentamycin (50 μg mL^{-1}), and spectinomycin (100 μg mL^{-1}), centrifuged, and resuspended in infiltration medium containing Silwet-77 (0.01% [v/v]) and benzylaminopurine (10 μg L^{-1}) as previously described (Bechtold and Pelletier, 1998). T1 seeds were collected, sterilized with ethanol, and sown on Murashige and Skoog plates containing glufosinate ammonium at 15 μg mL^{-1}. Approximately 60 independently transformed lines were selected based on their resistance, and the presence of single inserts was assessed in the T2 generation based on segregation analysis on glufosinate ammonium-Murashige and Skoog plates. Homozygous transformed lines bearing a single insert were grown under short-day conditions as described above and were harvested alongside wild-type plants for characterization of DXS enzyme activity in crude protein extracts. Lines constitutively expressing DXS with significantly higher activity compared with the wild type were selected for labeling experiments. For dark treatment, 1-month-old wild-type or DXS12 plants were placed in a lightproof container for 30 min at the midpoint of a 10-h photoperiod. Plants were harvested by flash freezing in liquid nitrogen.

Gas Exchange and Dynamic Labeling System

A LI-6400XT Portable Photosynthesis System (Li-Cor Biosciences) was used together with a custom-built Arabidopsis cuvette (Loivamäki et al., 2007) to

monitor and record gas exchange parameters in real time and to carry out $^{13}CO_2$ in vivo labeling under physiological conditions. Ambient air was conditioned by passing through a wash bottle and a CO_2 scrubber. CO_2 was maintained at a steady concentration with a supplemental CO_2 gas cartridge. The cuvette holds a single, full-size Arabidopsis rosette in a pot ($7 \times 7 \times 8$ cm) and delivers mixed air evenly across the leaf surface at a rate of 0.8 L min^{-1} with the assistance of an integrated mixing fan and a Peltier element that maintains temperature. Leaf temperature was monitored with a thermocouple touching the abaxial leaf surface. The total photosynthetically active plant surface area was estimated by photography of the plant together with a two-dimensional barcode size standard and automatic image analysis using PlantFriend, a software suite developed to detect the area of the size standard and the pixels representing the plant, which in turn is used to calculate the photosynthetically active plant surface area (http://www.plantviz.com). Light was provided by a 400-W high-pressure sodium lamp (Son-T Agro 400; Phillips) positioned above the cuvette at a distance giving 140 PPFD at the leaf surface, which was monitored with a LI-250 hand-held quantum sensor (Li-Cor Biosciences). Each individual plant was acclimated under standard conditions (21°C leaf temperature, 140 PPFD, 380 μmol mol^{-1} CO_2) for at least 30 min before the start of a labeling experiment. The pots and soil were wrapped in plastic wrap to prevent interference of soil respiration. Photosynthesis measurements were made according to the manufacturer's instructions using the stabilized CO_2 and water vapor exchange readings from the end of the acclimation period. The reference gas was measured using a portion of conditioned air diverted to the LI-6400XT before reaching the cuvette, whereas the sample gas was measured from the cuvette exhaust line connected to the same instrument.

In vivo labeling was accomplished by a single step change to a labeling atmosphere that was identical to the acclimation conditions except that all CO_2 was substituted by $^{13}CO_2$ (>99 atom % ^{13}C; Linde). Atmospheric replacement rates were calculated by monitoring the disappearance of CO_2 due to the relatively poor sensitivity of infrared gas analyzer CO_2 sensors to $^{13}CO_2$ (less than 33% signal relative to $^{12}CO_2$). Labeling times were calculated from the point at which one-half of the $^{12}CO_2$ signal had decayed. At the conclusion of a predetermined labeling period, the plant was quickly cut across the crown and its aerial portion was flash frozen in liquid nitrogen. Each labeled plant was ground to a fine powder in liquid nitrogen and lyophilized to dryness prior to analysis of label incorporation and characterization of DXS activity. Labeling experiments were restricted to a time period of at least 3 h after the start of the light phase and 2 h before darkness in order to eliminate any influence of a diurnal rhythm, which has been described for the MEP pathway (Covington et al., 2008; Wiberley et al., 2009).

Quantification of MEP Pathway Intermediates and DXP and MEcDP Label Incorporation Measurements

Lyophilized plant material (5 mg) was extracted twice with a 250-μL solution of 50% (v/v) acetonitrile containing 5 mM ammonium acetate, pH 9.0, by vortexing for 5 min, and was then centrifuged in a microcentrifuge. Two hundred μL from each extraction was pooled in a new 1.5-mL Eppendorf tube and dried under a stream of nitrogen gas at 40°C. The residue was dissolved in 100 μL of aqueous 10 mM ammonium acetate, pH 9.0, and transferred to a new Eppendorf tube. After extracting the solution with 100 μL of chloroform and separating the phases by centrifugation, the upper aqueous phase was transferred to a new Eppendorf tube and diluted with 1 volume of acetonitrile. After centrifugation for 5 min in a microcentrifuge to remove any precipitate, the supernatant was transferred to an HPLC vial.

The quantities of DXP and MEcDP metabolites and their ^{13}C incorporation were analyzed on an Agilent 1200 HPLC system (Agilent Technologies) connected to an API 5000 triple quadrupole mass spectrometer (AB Sciex). For separation, a ZIC-pHILIC column (5 μm, 150 $\times$ 2.1 mm; Merck) with a guard column containing the same sorbent (5 μm, 20 $\times$ 2.1 mm) was used. The solvents used were 20 mM ammonium acetate, pH 10.0, as solvent A and 80% (v/v) acetonitrile containing 20 mM ammonium acetate, pH 10.0, as solvent B; pH adjustments were made with liquid chromatography-mass spectrometry-grade ammonium hydroxide. Separation was achieved with a flow rate of 400 μL min^{-1} and a column temperature of 25°C. The solvent gradient profile started with an initial isocratic separation of 2 min at 100% B, followed by a isocratic separation of 13 min at 10% A, a wash step of 10 min at 40% A, and a return to initial conditions and 10 min of further equilibration. The volume injected was 1 μL. The mass spectrometer was used in negative ionization mode with the following instrument settings: ion spray voltage −4,500 V, turbo gas temperature 700°C, nebulizer gas 70 pounds per square inch (psi), heating gas 30 psi, curtain gas 30 psi, and collision gas 10 psi. Scheduled MRM was used to monitor the following precursor ion → product ion reactions: mass-to-charge ratio (*m/z*) 212.95 → 96.9, *m/z* 213.95 → 96.9, *m/z* 214.95 → 96.9, *m/z* 215.95 → 96.9, *m/z* 216.95 → 96.9, and *m/z* 217.95 → 96.9 for DXP containing 0, 1, 2, 3, 4, or 5 ^{13}C atoms respectively (collision energy [CE], −16 V; declustering potential [DP], −60 V; and cell exit potential [CXP], −15 V). MEcDP and its isotope distribution were monitored by the following precursor ion → product ion reactions: *m/z* 276.96 → 78.9, *m/z* 277.96 → 78.9, *m/z* 278.96 → 78.9, *m/z* 279.96 → 78.9, *m/z* 280.96→ 78.9, and *m/z* 281.96 → 78.9 (CE, −40 V; DP, −150 V; and CXP, −15 V). Both Q1 and Q2 quadrupoles were maintained at high resolution. Analyst 1.5 software (AB Sciex) was used for data acquisition and processing.

The DXP and MEcDP contents in plant extracts were quantified using external standard curves and were normalized to unlabeled DXP (Sigma) and MEcDP (Echelon Biosciences) standards added to each extract, after correction for natural ^{13}C abundance. Normalization to added unlabeled standards was accomplished by analyzing each plant sample twice, once with and once without the addition of 25-ng of DXP and 100-ng of MEcDP standards dissolved in 10 μL of water. The internal standard was added directly after the first extraction solvent was added to the dried plant material, and the absolute quantities of the metabolites in the plant extracts were calculated as described for DMADP quantification.

Analysis of DMADP

^{13}C incorporation into DMADP was measured by the acid-catalyzed hydrolysis of DMADP to isoprene, which was then analyzed by positive chemical ionization gas chromatography-mass spectrometry (GC-MS). The acid hydrolysis of 20 mg of lyophilized leaf material was performed as described by Brüggemann and Schnitzler (2002). The isoprene produced in the head space of a 2-mL airtight vial was measured with an Agilent 6890 Series gas chromatograph coupled to an Agilent 5973 quadrupole mass selective detector using positive-ion chemical ionization with methane as the reagent gas. The headspace was sampled with an airtight syringe, and 500 μL of air was injected into a programmable temperature vaporizing inlet (CIS 4; Gerstel) at 80°C containing a liner filled with Carbopack X adsorbent (Sigma-Aldrich). The contaminating CO_2 and water vapor were removed by venting for 1 min at a flow of 100 mL min^{-1}, after which the adsorbed isoprene was injected onto the capillary column held at 45°C while rapidly heating the liner to 240°C. The isoprene was then separated on an Al_2O_3/KCl column (25 m $\times$ 0.25 mm i.d. and film thickness 4 μm; Varian) using a temperature program starting at 45°C for 4 min, increasing at 15°C min^{-1} to 170°C and then at 40°C min^{-1} to 200°C, and then kept at 200°C for another 2 min. The carrier gas was helium with a flow rate of 0.5 mL min^{-1}. The mass spectrometry conditions were as follows: interface temperature 320°C, methane pressure 19 pounds per square inch gage, electron energy 68.1 eV, source temperature 150°C, quadrupole temperature 106°C, and scan range from 45 to 100 D. The calculation of exact labeling in isoprene is complicated by hydride abstraction and charge exchange in the analysis chamber of the mass selective detector, as explained in detail in the Supplemental Methods S1.

Mevalonic Acid Label Incorporation Measurements

Mevalonic acid was extracted from 50 mg of lyophilized plant material with 2 mL of extraction solvent prepared by adding 0.2 mL of 37% (v/v) HCl to 1.8 mL of 0.5 M KCl. The extract was vortexed for 5 min and then incubated at room temperature for another hour. After centrifugation, 1.8 mL of the supernatant was transferred to a new test tube and extracted three times with 1 mL of ethyl acetate. The ethyl acetate extracts were pooled and evaporated under a stream of nitrogen at 30°C. The resulting residue was dissolved in 1 mL of 2.5% (v/v) NH_4OH and incubated at room temperature for 1 h. This solution was then passed through an Oasis HLB SPE column (3 mL, 60 mg; Waters), conditioned with 3 mL of methanol and equilibrated with 3 mL of water and then 3 mL of 2.5% (v/v) NH_4OH. The flow-through was then loaded on an Oasis MAX SPE column (3 mL, 60 mg) conditioned and equilibrated as described for the HLB column. The Oasis MAX column was then washed with 1.5 mL of 2.5% (v/v) NH_4OH and 1.5 mL of methanol, and then eluted with 1 mL of methanol containing 2% (v/v) formic acid. The eluate was then dried under a stream of nitrogen at 30°C and the residue dissolved in 50 μL of 2.5% (v/v) NH_4OH and incubated overnight at 4°C. The next day, 50 μL of acetonitrile was added, and the solution was centrifuged at maximum speed in a microcentrifuge for 5 min. Finally, the supernatant was transferred to a HPLC vial for analysis.

The mevalonic acid content and its isotope distribution were analyzed on an Agilent 1200 HPLC system connected to an API 5000 triple quadrupole mass spectrometer. For separation, an XBridge Amide column (3.5 μm, 150 × 2.1 mm; Waters) with a guard column containing the same sorbent (3.5 μm, 10 × 2.1 mm) was employed. The solvents used were 10 mM ammonium acetate adjusted to pH 9.0 with liquid chromatography-mass spectrometry-grade NH_4OH as solvent A and 90% (v/v) acetonitrile containing 10 mM ammonium acetate, pH 9.0, as solvent B. Separation was achieved with a flow rate of 500 μL min^{-1} and a column temperature of 25°C. The solvent gradient profile started with a linear gradient from 0% A to 30% A over 20 min, followed by a wash step at 45% A for 5 min, and a return to 0% A and 5 min of further equilibration. The volume injected was 5 μL. The mass spectrometer was used in negative ionization mode with the following instrument settings: ion spray voltage 2,500 V, turbo gas temperature 700°C, nebulizer gas 70 psi, heating gas 70 psi, curtain gas 25 psi, and collision gas 10 psi. MRM was used to monitor the following precursor ion → product ion reactions: *m/z* 146.97 → 58.8, *m/z* 147.97 → 59.8, *m/z* 148.97 → 58.8, *m/z* 148.97 → 60.8, *m/z* 149.97 → 59.8, *m/z* 149.97 → 60.8, *m/z* 150.97 → 60.8, *m/z* 151.97→ 59.8, *m/z* 151.97 → 60.8, and *m/z* 152.97 → 60.8 (CE, −18 V; DP, −55 V; and CXP, −9 V). Because the product ion contained two carbon atoms, multiple precursor ion → product ion combinations were used to quantify each precursor ion mass that contained more than two ^{13}C atoms. Due to low signal intensity and high background, not all of the precursor ion → product ion scan combinations necessary to determine the complete isotope distribution of mevalonic acid could be measured. Both Q1 and Q2 quadrupoles were maintained at high resolution. Analyst 1.5 software was used for data acquisition and processing.

Determination of Flux by Label Incorporation

Fluxes in the MEP pathway in wild-type, mutant, and transgenic lines were calculated from the absolute ^{13}C incorporation into DXP in time course labeling assays ranging from 6 to 60 min. $^{13}CO_2$ labeling was initiated only after a greater than 30-min adaptation phase once plants had reached a photosynthetic steady state according to gas exchange measurements. For each line, 10 to 20 individual plants were labeled in time course experiments. The total labeled fraction of DXP was calculated using the m_0 through m_5 molecular ion species obtained from LC-MS/MS analysis according to the equation $(1/N)\ \sum_{i=1}^{N} M_i \times i$ (Young et al., 2011), where N is the number of carbon atoms in the molecule and M_i is the fractional abundance of the ith isotopologue. The isotopologues are represented by m_n with n being the number of ^{13}C atoms incorporated. Natural abundances of ^{13}C, ^{17}O, and ^{18}O were measured in unlabeled standards and subtracted from labeled sample mass spectra to determine exact ^{13}C amounts introduced during labeling. After plotting corrected labeling time against total fraction labeled, data were fitted to curves as the exponential rise to maximum, according to the equation $A \times (1 - e^{[-k \times t]})$, where A is the labeling plateau, t is the labeling time, and k is the kinetic rate constant. Equations were fitted to the time course data for each plant line by iteratively adjusting A and k to minimize χ^2 values using the Levenberg-Marquardt minimization algorithm as implemented in the SciPy library of scientific computational routines (http://www.scipy.org). Seed estimates were obtained by visual inspection of the labeling maxima of the curves (for A), and by using $1/t_{1/2}$ (for k). The flux was then calculated for each line by multiplying the DXP pool size by the fitted rate constant k.

DXS Enzyme Assay

To quantify DXS activity in labeled plants, enzyme activities were measured in total protein extracts of lyophilized tissues under saturating substrate conditions. Except where otherwise indicated, all reagents were purchased from Sigma-Aldrich. Crude enzyme extracts were made from 5 mg of lyophilized plant material as described above. Care was taken to store the dried plant material at −20°C and to keep samples on ice during the extraction procedure. Enzymes were extracted in 1 mL of extraction buffer at 4°C for 15 min by gently mixing the suspension on a vertical rotator (Stuart rotator SB3; VWR International) set at 20 rpm. The extraction buffer consisted of 50 mM Tris-HCl, pH 8.0, 10% (v/v) glycerol, 0.5% (v/v) Tween 20, 1% (w/v) polyvinylpyrrolidone (average M_r 360,000), 10 mM dithiothreitol, 1 mM ascorbic acid, 100 μM thiamine pyrophosphate, 1% (v/v) protease inhibitor cocktail for plant cell and tissue, 2 mM imidazole, 1 mM sodium fluoride, and 1.15 mM molybdate. The enzyme extract was then centrifuged at 16,000*g* for 20 min at 4°C in a microcentrifuge. The DXS assay mixture consisted of 50 mM Tris-HCl, pH 8.0, 10% (v/v) glycerol, 10 mM $MgCl_2$, 2.5 mM dithiothreitol, 1 mM thiamine pyrophosphate, 2 mM imidazole, 1 mM sodium fluoride, 1.15 mM molybdate, 1% (v/v) protease inhibitor cocktail, and 10 mM each of the substrates pyruvate and G3P. The enzyme reaction was started by the addition of 30 μL of enzyme extract in a final volume of 100 μL and incubated in a water bath at 25°C for 2 h. The enzyme reaction was stopped by vigorously vortexing for 5 s with 100 μL of chloroform. After centrifugation in a microcentrifuge to achieve phase separation, a portion of the aqueous phase was removed and diluted 1:10 with 10 ng μL^{-1} [3,4,5-$^{13}C_3$] DXP dissolved in water as an internal standard. The enzymatic end product DXP was then quantified relative to the internal standard using LC-MS/MS analysis.

Analysis of DXP was carried out on an Agilent 1200 HPLC system (Agilent Technologies) connected to an API 3200 triple quadrupole mass spectrometer (AB Sciex). For separation, a Nucleodex β-OH column (particle size 5 μm, column dimensions 200 × 4 mm; Macherey-Nagel) with a guard column containing the same sorbent (particle size 5 μm, column dimensions 30 × 4 mm) was used. The solvents used were 10 mM ammonium acetate as solvent A and acetonitrile as solvent B. Separation was achieved with a flow rate of 1 mL min^{-1} and a column temperature of 25°C. The solvent gradient profile started with an initial isocratic separation of 5 min at 10% A, followed by a linear gradient of 10 min to 50% A, a wash step of 5 min at 50% A, and a return to initial conditions and 10 min of further equilibration. The volume injected was 20 μL. The mass spectrometer was used in negative ionization mode with the following instrument settings: ion spray voltage −4,200 V, turbo gas temperature 700°C, nebulizer gas 70 psi, heating gas 70 psi, curtain gas 20 psi, and collision gas 5 psi. MRM was used to monitor losses of the following: *m/z* 212.9 → 138.9 precursor ion → product ion for enzymatically produced DXP and *m/z* 215.9 → 140.9 for the isotopically labeled DXP internal standard (CE, −18 V; DP, −20 V; and CXP, −8 V). MRM was also used to monitor losses of: *m/z* 212.9 → 78.9 and *m/z* 215.9 → 78.9 for the enzymatic DXP and internal standard, respectively (CE, −42 V; DP, −20 V; and CXP, −7 V). Both Q1 and Q2 quadrupoles were maintained at unit resolution. Analyst version 1.5 software (AB Sciex) was used for data acquisition and processing. The DXP produced by the DXS enzyme reaction was quantified using external standard curves and was normalized to the [$^{13}C_3$]-DXP internal standard.

Calculation of Metabolic Control Coefficients

Control coefficients were estimated from the general formula $C_v^y = \frac{dy/y}{dv/v} = \frac{dy}{dv} \cdot \frac{v}{y}$ where C_v^y is the control coefficient, y is the variable of interest (flux or metabolite pool concentration), and v is the DXS enzyme activity (determined as described). Data from the wild type and DXS transgenic plants were combined, and the term dy/dv was obtained from linear regression of a plot of the variable of interest (flux, DXP, MEcDP, or DMADP concentration) against DXS activity. The linear nature of the data allowed this approximation to be made ($R^2 > 0.9$). The slope was scaled by the v/y values for the wild-type plant. Deviation indices for these data were calculated as described (Small and Kacser, 1993). Elasticity (ε) of DXS for DMADP was calculated by measuring DXS activity in total protein extracts of wild-type Arabidopsis after the addition of different concentrations of DMADP (0–15 μM). A linear regression of DXS activity versus exogenously added DMADP concentration was determined for this purpose and scaled as described above. For these assays, the physiologically relevant concentrations of pyruvate (30 μM), G3P (70 μM), and thiamin pyrophosphate (100 μM) were used based on previous literature reports of pool size and compartmentation (Arrivault et al., 2009; Bocobza et al., 2013; Szecowka et al., 2013).

Quantitative Real-Time PCR Analysis of MEP Pathway Genes

RNA was extracted from tissue harvested from plants at noon using a QIAGEN Plant RNeasy extraction kit (Qiagen) with a QIAGEN on-column DNase digestion step. RNA samples were quantified using a NanodropND-1000. Complementary DNA (cDNA) was synthesized using a Roche Transcriptor First Strand cDNA Synthesis Kit according to the manufacturer's instructions. Transcript abundance was measured with SYBR green assays in a Roche LightCycler480 II using wild-type samples as a calibrator. cDNA loading was normalized to the ADENINE PHOSPHORIBOSYLTRANSFERASE1 (AT1G27450) and RNA POLYMERASE II LARGE SUBUNIT (At4g35800) genes. Primers were designed using Beacon Designer version 4.0 and efficiency was calculated for each primer pair as described (Pfaffl, 2001). Transcripts for all MEP pathway genes (Phillips et al., 2008) were measured in all lines and quantified relative to wild-type plants. Primer specificity was verified by sequencing cloned amplicons for each primer pair. Primer sequences are listed in Supplemental Table S2.

HPLC Analysis of Plant Pigments

Six plants from each transgenic, mutant, or wild-type line were grown under short-day conditions as described. Plants were harvested by flash freezing in liquid nitrogen, ground in a prechilled mortar and pestle, and lyophilized to dryness. Samples were protected from light and heat during these steps as well as during subsequent extraction. Prior to lyophilization, an aliquot of fresh frozen tissue was set aside for RNA extraction. Pigment extractions were performed in triplicate on each individual plant (18 total extractions per line) using 4 mg of lyophilized plant tissue according to Fraser et al. (2000). Five micrograms of canthaxanthin (Sigma-Aldrich) was added as the internal standard. Chromatographic separations were performed using an Agilent 1200 HPLC equipped with a diode array detector and a YMC C30 column (25 cm × 4.6 mm i.d.; Waters) using the same solvent system described by Fraser et al. (2000). The quantification of chlorophyll *a* and *b* and α-tocopherol was done according to external standard curves using authentic standards. The concentrations of major carotenoids (violaxanthin, neoxanthin, lutein, β-carotene, and cis-β-carotene) were approximated using a calibration curve generated from a β-carotene standard. Results were expressed relative to the quantities in wild-type plants harvested on the same day.

Statistical Analysis

For statistical analysis, the software suites SigmaStat (Systat Software) and R (http://www.r-project.org) were used. Putative changes in the metabolic steady-state concentrations of metabolites during $^{13}CO_2$ labeling were evaluated by linear regression of metabolite levels plotted against labeling time. Differences in expression levels of MEP pathway genes in 35S:DXS lines, the *dxs3* mutant line, and wild-type plants were analyzed by paired *t* tests with cutoffs of $P = 0.05$ or $P = 0.01$. Incorporation of the $^{13}CO_2$ label into the MEP pathway intermediates DXP, MEcDP, and DMADP, as well as pigment levels in wild-type, DXS-overexpressing, and DXS mutant (*dxs3*) lines were compared by using the Student's *t* test. The significance of the correlations between DXS activity and photosynthesis, flux, and DXP, MEcDP, and DMADP pool size was tested by linear regression analysis.

Sequence data from this article can be found in the GenBank/EMBL data libraries under accession numbers *DXS* (AT4G15560), *DXR* (AT5G62790), *MCT* (AT2G02500), *CMK* (AT2G26930), *MDS* (AT1G63970), *HDS* (AT5G60600), *HDR* (AT4G34350), *AOS* (AT5G42650) *ICS1* (AT1G74710), *HPL* (AT4G15440), *RP2ls* (At4g35800), and *APT1* (AT1G27450).

Supplemental Data

The following materials are available in the online version of this article.

Supplemental Figure S1. Analysis of $^{13}CO_2$ label incorporation into mevalonate in extracts of illuminated Arabidopsis rosettes.

Supplemental Figure S2. DXS enzyme assay optimization.

Supplemental Figure S3. DXS activity in total protein extracts of wild-type, transgenic 35S:DXS, and *dxs3* mutant lines.

Supplemental Figure S4. Elasticity of DXS for DMADP.

Supplemental Table S1. Calculation of deviation indices in DXS-altered lines relative to a wild-type reference state.

Supplemental Table S2. Quantitative PCR primer sequences used in this study.

Supplemental Methods S1. Calculation of exact label incorporation into DMADP detected as isoprene gas.

Received June 16, 2014; accepted June 26, 2014; published July 1, 2014.

LITERATURE CITED

Affek HP, Yakir D (2003) Natural abundance carbon isotope composition of isoprene reflects incomplete coupling between isoprene synthesis and photosynthetic carbon flow. Plant Physiol **131:** 1727–1736

Allen DK, Laclair RW, Ohlrogge JB, Shachar-Hill Y (2012) Isotope labelling of Rubisco subunits provides in vivo information on subcellular biosynthesis and exchange of amino acids between compartments. Plant Cell Environ **35:** 1232–1244

Alonso AP, Dale VL, Shachar-Hill Y (2010) Understanding fatty acid synthesis in developing maize embryos using metabolic flux analysis. Metab Eng **12:** 488–497

Andrews TJ, Kane HJ (1991) Pyruvate is a by-product of catalysis by ribulosebisphosphate carboxylase/oxygenase. J Biol Chem **266:** 9447–9452

Araki N, Kusumi K, Masamoto K, Niwa Y, Iba K (2000) Temperature-sensitive *Arabidopsis* mutant defective in 1-deoxy-D-xylulose 5-phosphate synthase within the plastid non-mevalonate pathway of isoprenoid biosynthesis. Physiol Plant **108:** 19–24

Arrivault S, Guenther M, Ivakov A, Feil R, Vosloh D, van Dongen JT, Sulpice R, Stitt M (2009) Use of reverse-phase liquid chromatography, linked to tandem mass spectrometry, to profile the Calvin cycle and other metabolic intermediates in *Arabidopsis* rosettes at different carbon dioxide concentrations. Plant J **59:** 826–839

Banerjee A, Wu Y, Banerjee R, Li Y, Yan H, Sharkey TD (2013) Feedback inhibition of deoxy-D-xylulose-5-phosphate synthase regulates the methylerythritol 4-phosphate pathway. J Biol Chem **288:** 16926–16936

Bechtold N, Pelletier G (1998) In planta *Agrobacterium*-mediated transformation of adult *Arabidopsis thaliana* plants by vacuum infiltration. Methods Mol Biol **82:** 259–266

Bick JA, Lange BM (2003) Metabolic cross talk between cytosolic and plastidial pathways of isoprenoid biosynthesis: unidirectional transport of intermediates across the chloroplast envelope membrane. Arch Biochem Biophys **415:** 146–154

Bocobza SE, Malitsky S, Araújo WL, Nunes-Nesi A, Meir S, Shapira M, Fernie AR, Aharoni A (2013) Orchestration of thiamin biosynthesis and central metabolism by combined action of the thiamin pyrophosphate riboswitch and the circadian clock in *Arabidopsis*. Plant Cell **25:** 288–307

Bouvier F, Rahier A, Camara B (2005) Biogenesis, molecular regulation and function of plant isoprenoids. Prog Lipid Res **44:** 357–429

Brüggemann N, Schnitzler JP (2002) Diurnal variation of dimethylallyl diphosphate concentrations in oak (*Quercus robur*) leaves. Physiol Plant **115:** 190–196

Carretero-Paulet L, Cairó A, Botella-Pavía P, Besumbes O, Campos N, Boronat A, Rodríguez-Concepción M (2006) Enhanced flux through the methylerythritol 4-phosphate pathway in *Arabidopsis* plants overexpressing deoxyxylulose 5-phosphate reductoisomerase. Plant Mol Biol **62:** 683–695

Colón AM, Sengupta N, Rhodes D, Dudareva N, Morgan J (2010) A kinetic model describes metabolic response to perturbations and distribution of flux control in the benzenoid network of *Petunia hybrida*. Plant J **62:** 64–76

Covington MF, Maloof JN, Straume M, Kay SA, Harmer SL (2008) Global transcriptome analysis reveals circadian regulation of key pathways in plant growth and development. Genome Biol **9:** R130

Croteau R (1987) Biosynthesis and catabolism of monoterpenoids. Chem Rev **87:** 929–954

Dudareva N, Andersson S, Orlova I, Gatto N, Reichelt M, Rhodes D, Boland W, Gershenzon J (2005) The nonmevalonate pathway supports both monoterpene and sesquiterpene formation in snapdragon flowers. Proc Natl Acad Sci USA **102:** 933–938

Estévez JM, Cantero A, Reindl A, Reichler S, León P (2001) 1-Deoxy-D-xylulose-5-phosphate synthase, a limiting enzyme for plastidic isoprenoid biosynthesis in plants. J Biol Chem **276:** 22901–22909

Fell D (1997) Understanding the Control of Metabolism: Frontiers in Metabolism, **Vol 2**. Portland Press, London

Fell DA (1992) Metabolic control analysis: a survey of its theoretical and experimental development. Biochem J **286:** 313–330

Fell DA (2005) Enzymes, metabolites and fluxes. J Exp Bot **56:** 267–272

Flores-Pérez U, Sauret-Güeto S, Gas E, Jarvis P, Rodríguez-Concepción M (2008) A mutant impaired in the production of plastome-encoded proteins uncovers a mechanism for the homeostasis of isoprenoid biosynthetic enzymes in *Arabidopsis* plastids. Plant Cell **20:** 1303–1315

Flügge UI, Gao W (2005) Transport of isoprenoid intermediates across chloroplast envelope membranes. Plant Biol (Stuttg) **7:** 91–97

Fraser PD, Pinto MES, Holloway DE, Bramley PM (2000) Technical advance: application of high-performance liquid chromatography with photodiode array detection to the metabolic profiling of plant isoprenoids. Plant J **24:** 551–558

Furumoto T, Yamaguchi T, Ohshima-Ichie Y, Nakamura M, Tsuchida-Iwata Y, Shimamura M, Ohnishi J, Hata S, Gowik U, Westhoff P, et al (2011) A plastidial sodium-dependent pyruvate transporter. Nature **476:** 472–475

Gershenzon J, Dudareva N (2007) The function of terpene natural products in the natural world. Nat Chem Biol **3:** 408–414

Ghirardo A, Gutknecht J, Zimmer I, Brüggemann N, Schnitzler JP (2011) Biogenic volatile organic compound and respiratory CO_2 emissions after ^{13}C-labeling: online tracing of C translocation dynamics in poplar plants. PLoS ONE **6:** e17393

Ghirardo A, Wright LP, Bi Z, Rosenkranz M, Pulido P, Rodríguez-Concepción M, Niinemets Ü, Brüggemann N, Gershenzon J, Schnitzler JP (2014) Metabolic flux analysis of plastidic isoprenoid biosynthesis in poplar leaves emitting and nonemitting isoprene. Plant Physiol **165:** 37–51

Gil MJ, Coego A, Mauch-Mani B, Jordá L, Vera P (2005) The *Arabidopsis csb3* mutant reveals a regulatory link between salicylic acid-mediated disease resistance and the methyl-erythritol 4-phosphate pathway. Plant J **44:** 155–166

Guevara-García A, San Román C, Arroyo A, Cortés ME, de la Luz Gutiérrez-Nava M, León P (2005) Characterization of the *Arabidopsis clb6* mutant illustrates the importance of posttranscriptional regulation of the methyl-D-erythritol 4-phosphate pathway. Plant Cell **17:** 628–643

Gutiérrez-Nava MdeL, Gillmor CS, Jiménez LF, Guevara-García A, León P (2004) CHLOROPLAST BIOGENESIS genes act cell and noncell autonomously in early chloroplast development. Plant Physiol **135:** 471–482

Hasunuma T, Harada K, Miyazawa S, Kondo A, Fukusaki E, Miyake C (2010) Metabolic turnover analysis by a combination of in vivo ^{13}C-labelling from $^{13}CO_2$ and metabolic profiling with CE-MS/MS reveals rate-limiting steps of the C3 photosynthetic pathway in *Nicotiana tabacum* leaves. J Exp Bot **61:** 1041–1051

Hemmerlin A, Hoeffler JF, Meyer O, Tritsch D, Kagan IA, Grosdemange-Billiard C, Rohmer M, Bach TJ (2003) Cross-talk between the cytosolic mevalonate and the plastidial methylerythritol phosphate pathways in tobacco bright yellow-2 cells. J Biol Chem **278:** 26666–26676

Joyard J, Ferro M, Masselon C, Seigneurin-Berny D, Salvi D, Garin J, Rolland N (2010) Chloroplast proteomics highlights the subcellular compartmentation of lipid metabolism. Prog Lipid Res **49:** 128–158

Kacser H, Burns JA (1995) The control of flux. Biochem Soc Trans **23:** 341–366

Karimi M, Inzé D, Depicker A (2002) GATEWAY vectors for *Agrobacterium*-mediated plant transformation. Trends Plant Sci **7:** 193–195

Kempa S, Hummel J, Schwemmer T, Pietzke M, Strehmel N, Wienkoop S, Kopka J, Weckwerth W (2009) An automated GCxGC-TOF-MS protocol for batch-wise extraction and alignment of mass isotopomer matrixes from differential ^{13}C-labelling experiments: a case study for photoautotrophic-mixotrophic grown *Chlamydomonas reinhardtii* cells. J Basic Microbiol **49:** 82–91

Knappe S, Flügge UI, Fischer K (2003) Analysis of the plastidic phosphate translocator gene family in Arabidopsis and identification of new phosphate translocator-homologous transporters, classified by their putative substrate-binding site. Plant Physiol **131:** 1178–1190

Kreuzwieser J, Graus M, Wisthaler A, Hansel A, Rennenberg H, Schnitzler JP (2002) Xylem-transported glucose as an additional carbon source for leaf isoprene formation in *Quercus robur*. New Phytol **156:** 171–178

Lange BM, Ahkami A (2013) Metabolic engineering of plant monoterpenes, sesquiterpenes and diterpenes—current status and future opportunities. Plant Biotechnol J **11:** 169–196

Laule O, Fürholz A, Chang HS, Zhu T, Wang X, Heifetz PB, Gruissem W, Lange M (2003) Crosstalk between cytosolic and plastidial pathways of isoprenoid biosynthesis in *Arabidopsis thaliana*. Proc Natl Acad Sci USA **100:** 6866–6871

Li Z, Sharkey TD (2013) Metabolic profiling of the methylerythritol phosphate pathway reveals the source of post-illumination isoprene burst from leaves. Plant Cell Environ **36:** 429–437

Loivamäki M, Louis S, Cinege G, Zimmer I, Fischbach RJ, Schnitzler JP (2007) Circadian rhythms of isoprene biosynthesis in grey poplar leaves. Plant Physiol **143:** 540–551

Magel E, Mayrhofer S, Muller A, Zimmer I, Hampp R, Schnitzler JP (2006) Photosynthesis and substrate supply for isoprene biosynthesis in poplar leaves. Atmos Environ (Suppl 1) **40:** 138–151

Mongélard G, Seemann M, Boisson AM, Rohmer M, Bligny R, Rivasseau C (2011) Measurement of carbon flux through the MEP pathway for isoprenoid synthesis by ^{31}P-NMR spectroscopy after specific inhibition of 2-C-methyl-d-erythritol 2,4-cyclodiphosphate reductase. Effect of light and temperature. Plant Cell Environ **34:** 1241–1247

Nogués I, Brilli F, Loreto F (2006) Dimethylallyl diphosphate and geranyl diphosphate pools of plant species characterized by different isoprenoid emissions. Plant Physiol **141:** 721–730

Pfaffl MW (2001) A new mathematical model for relative quantification in real-time RT-PCR. Nucleic Acids Res **29:** e45

Phillips MA, León P, Boronat A, Rodríguez-Concepción M (2008) The plastidial MEP pathway: unified nomenclature and resources. Trends Plant Sci **13:** 619–623

Prabhakar V, Löttgert T, Gigolashvili T, Bell K, Flügge UI, Häusler RE (2009) Molecular and functional characterization of the plastid-localized Phosphoenolpyruvate enolase (ENO1) from *Arabidopsis thaliana*. FEBS Lett **583:** 983–991

Pulido P, Toledo-Ortiz G, Phillips MA, Wright LP, Rodríguez-Concepción M (2013) *Arabidopsis* J-protein J20 delivers the first enzyme of the plastidial isoprenoid pathway to protein quality control. Plant Cell **25:** 4183–4194

Ramos-Valdivia AC, van der Heijden R, Verpoorte R (1997) Isopentenyl diphosphate isomerase: a core enzyme in isoprenoid biosynthesis. A review of its biochemistry and function. Nat Prod Rep **14:** 591–603

Rivasseau C, Seemann M, Boisson AM, Streb P, Gout E, Douce R, Rohmer M, Bligny R (2009) Accumulation of 2-C-methyl-D-erythritol 2,4-cyclodiphosphate in illuminated plant leaves at supraoptimal temperatures reveals a bottleneck of the prokaryotic methylerythritol 4-phosphate pathway of isoprenoid biosynthesis. Plant Cell Environ **32:** 82–92

Rodríguez-Concepción M, Forés O, Martinez-García JF, González V, Phillips MA, Ferrer A, Boronat A (2004) Distinct light-mediated pathways regulate the biosynthesis and exchange of isoprenoid precursors during *Arabidopsis* seedling development. Plant Cell **16:** 144–156

Rohwer JM (2012) Kinetic modelling of plant metabolic pathways. J Exp Bot **63:** 2275–2292

Ruiz-Sola MA, Rodríguez-Concepción M (2012) Carotenoid biosynthesis *in Arabidopsis*: a colorful pathway. Arabidopsis Book **10:** e0158, doi/10.1199/tab.0158

Schnitzler JP, Graus M, Kreuzwieser J, Heizmann U, Rennenberg H, Wisthaler A, Hansel A (2004) Contribution of different carbon sources to isoprene biosynthesis in poplar leaves. Plant Physiol **135:** 152–160

Sharkey TD, Loreto F, Delwiche CF (1991) High-carbon dioxide and sun/shade effects on isoprene emission from oak and aspen tree leaves. Plant Cell Environ **14:** 333–338

Sharkey TD, Monson RK (2014) The future of isoprene emission from leaves, canopies and landscapes. Plant Cell Environ

Shastri AA, Morgan JA (2007) A transient isotopic labeling methodology for ^{13}C metabolic flux analysis of photoautotrophic microorganisms. Phytochemistry **68:** 2302–2312

Small JR, Kacser H (1993) Responses of metabolic systems to large changes in enzyme activities and effectors. 1. The linear treatment of unbranched chains. Eur J Biochem **213:** 613–624

Stitt M, Ap Rees T (1979) Capacities of pea chloroplasts to catalyse the oxidative pentose phosphate pathway and glycolysis. Phytochemistry **18:** 1905–1911

Szecowka M, Heise R, Tohge T, Nunes-Nesi A, Vosloh D, Huege J, Feil R, Lunn J, Nikoloski Z, Stitt M, et al (2013) Metabolic fluxes in an illuminated *Arabidopsis* rosette. Plant Cell **25:** 694–714

Tambasco-Studart M, Titiz O, Raschle T, Forster G, Amrhein N, Fitzpatrick TB (2005) Vitamin B6 biosynthesis in higher plants. Proc Natl Acad Sci USA **102:** 13687–13692

Trowbridge AM, Asensio D, Eller ASD, Way DA, Wilkinson MJ, Schnitzler JP, Jackson RB, Monson RK (2012) Contribution of various carbon sources toward isoprene biosynthesis in poplar leaves mediated by altered atmospheric CO_2 concentrations. PLoS ONE **7:** e32387

Voll L, Häusler RE, Hecker R, Weber A, Weissenböck G, Fiene G, Waffenschmidt S, Flügge UI (2003) The phenotype of the *Arabidopsis cue1* mutant is not simply caused by a general restriction of the shikimate pathway. Plant J **36:** 301–317

Ward JL, Baker JM, Llewellyn AM, Hawkins ND, Beale MH (2011) Metabolomic analysis of *Arabidopsis* reveals hemiterpenoid glycosides as products of a nitrate ion-regulated, carbon flux overflow. Proc Natl Acad Sci USA **108:** 10762–10767

Weise SE, Li Z, Sutter AE, Corrion A, Banerjee A, Sharkey TD (2013) Measuring dimethylallyl diphosphate available for isoprene synthesis. Anal Biochem **435:** 27–34

Wiberley AE, Donohue AR, Westphal MM, Sharkey TD (2009) Regulation of isoprene emission from poplar leaves throughout a day. Plant Cell Environ **32:** 939–947

Williams TCR, Miguet L, Masakapalli SK, Kruger NJ, Sweetlove LJ, Ratcliffe RG (2008) Metabolic network fluxes in heterotrophic Arabidopsis cells: stability of the flux distribution under different oxygenation conditions. Plant Physiol **148:** 704–718

Xiao Y, Savchenko T, Baidoo EEK, Chehab WE, Hayden DM, Tolstikov V, Corwin JA, Kliebenstein DJ, Keasling JD, Dehesh K (2012) Retrograde signaling by the plastidial metabolite MEcPP regulates expression of nuclear stress-response genes. Cell **149:** 1525–1535

Young JD, Shastri AA, Stephanopoulos G, Morgan JA (2011) Mapping photoautotrophic metabolism with isotopically nonstationary $^{(13)}C$ flux analysis. Metab Eng **13:** 656–665

Zhou K, Zou R, Stephanopoulos G, Too H-P (2012) Metabolite profiling identified methylerythritol cyclodiphosphate efflux as a limiting step in microbial isoprenoid production. PLoS ONE **7:** e47513